Development of Modular Polymeric NPs for Drug Delivery Using Amine-Reactive Chemistry

by

Calvin Wong

A thesis

presented to the University of Waterloo

in fulfillment of the

thesis requirement for the degree of

Master of Science

in

Pharmacy

Waterloo, Ontario, Canada, 2024

Author's Declaration

This thesis consists of material all of which I authored or co-authored: see Statement of Contributions included in the thesis. This is a true copy of the thesis, including any required final revisions, as accepted by my examiners.

I understand that my thesis may be made electronically available to the public.

Statement of Contributions

Calvin Wong was the sole author of Chapters 1, 2, 4, which were written under the supervision of Dr. Emmanuel Ho.

RE: Chapter 3

Experimental studies were conducted by Calvin Wong under supervision of Dr. Emmanuel Ho; select experimental protocols were adapted from related work and consultation by Dr. Yannick Traore, Jin Wang and Sihan Dong. Experimental work was conducted by Calvin Wong. Some heavy equipment data (Nuclear Magnetic Resonance, MALDI-TOF Mass Spectrometry) was collected with assistance from research technicians, Dr. Blossom Yan and Valerie Goodfellow, respectively.

Abstract

Cancer remains one of the leading causes of death worldwide and very often requires chemotherapy treatment. Despite advances in chemotherapy treatments, some cancers remain difficult to treat due to tumour type, location, and in some cases, the development of drug resistances. In order to tackle cancer more effectively, researchers have explored and developed novel chemotherapy agents. However, many of these agents suffer from low bioavailability or prohibitively high toxicity to the body. Nanotechnology-based drug delivery systems aim to assist in protection and site-specific delivery of these potential anti-cancer agents, increasing their effectiveness and lowering toxic effects. Polymeric NP delivery systems can encapsulate drugs and be coated with functional groups or moieties to enhance various properties such as targeting.

In this project, poly(lactic-co-glycolic) acid (PLGA) NPs were synthesized to encapsulate curcumin (CUR) via single emulsion method. CUR, the principal constituent of *Curcuma longa*, commonly known as turmeric, has been explored for its anti-cancer potential, but is severely limited by its hydrophobicity and sensitivity to light and water. The PLGA NPs were coated with oligomeric chitosan (COS) and RGD peptide (peptide consisting of Arg-Gly-Asp) using amine-reactive chemistry (NHS and EDC). Both COS and RGD had been previously shown to accumulate and target many different types of cancer cells. NPs were characterised based on size distribution, zeta potential, and binding efficiency of RGD peptide. They were also evaluated on encapsulation efficiency, and stability, of CUR within the NPs. OVCAR-3 cancer cells were treated with COS and RGD-coated PLGA NPs loaded with Coumarin-6 dye for fluorescent imaging of cell uptake. They were also treated with CUR-loaded NPs to determine cytotoxicity and effectiveness of delivery.

The NPs exhibited size distribution and zeta potential within expected values, though binding efficiency of RGD was low. CUR-loaded NPs showed significant increase in cytotoxicity over free (unencapsulated) CUR, and void (empty) NPs, suggesting successful delivery of CUR as an anti-cancer agent; the performance of COS and RGD coated NPs over bare PLGA NPs was inconclusive, however.

Optimization will be required to improve formulation during the coating steps. Further investigation may be required into alternative binding chemistry, such as click chemistry.

Acknowledgements

I would like to thank my supervisor Dr. Emmanuel Ho for his support, guidance, and encouragement over my years of study. I would also like to thank my advisory committee members, Dr. Praveen Rao Perampalli Nekkar and Dr. Scott Taylor for their insights throughout this process.

I am grateful to my lab mates and the members of the Ho Research Group: Dr. Yannick Traore, Jin Wang, Dr. Chen Sun, Chuying Feng, Derek Chen, Sihan Dong, Alistair Chen, Ethan Watt, Ryan Nodder, and Kaidy Orellena, for their support, their encouragement, and most importantly, their friendship. It was a pleasure to work and laugh alongside them; I owe much to their moral support, words of kindness, and insights during times of difficulty. In particular, I would like to thank Dr. Traore, Jin and Sihan, as well as our School of Pharmacy research technician, Dr. Monica Tudorancea, for their direct assistance in several aspects of this project, and for their knowledge and patience to help teach me essential techniques to not only this project, but to many general techniques crucial to a proper, safe, functioning lab. I would like to thank the Nuclear Magnetic Resonance technician, Dr. Blossom Yan, for her expertise to teach me the practical ins and outs of using and operating Nuclear Magnetic Resonance equipment properly.

Finally, I would like to thank my friends and loving family for providing me such support; without them, I would not be where I am today, as the person I am today. I know they have and will continue to shape my life for the better, through this program and beyond.

Table of Contents

List of Figures

List of Tables

Table of Abbreviations

- ACN ..... Acetonitrile
- ANOVA ..... Analysis of variance
- BCA ..... Bicinchoninic acid
- COS ..... Chitooligosaccharide
- CUR ..... Curcumin
- DAPI ..... 4’,6-diamidino-2-phenylindole
- DL ..... Drug loading
- ECM ..... Extracellular matrix
- EDC ..... N-(3-Dimethylaminopropyl)-N'-ethylcarbodiimide hydrochloride
- EE ..... Encapsulation efficiency
- HPLC/UPLC ..... High/Ultra Performance Liquid Chromatography
- MALDI-TOF ..... Matrix assisted laser desorption ionization time of flight
- MES ..... 4-morpholineethanesulfonic acid
- MS ..... Mass spectrometry
- NHS ..... N-hydroxysuccinimide
- NMR ..... Nuclear Magnetic Resonance (spectroscopy)
- NP ..... Nanoparticle
- PDA ..... Photodiode array
- PDI ..... Polydispersity index
- PEG ..... Poly(ethylene glycol)
- PGA ..... Poly-glycolic acid
- PLA ..... Poly-lactic acid
- PLGA ..... Poly(lactic-co-glycolic) acid
- RGD ..... Arg-Gly-Asp
- TNBS ..... 2,4,6-trinitrobenzene sulfonic acid
- T-80 ..... Tween-80
- UPLC ..... Ultra performance liquid chromatography
- ZP ..... Zeta potential

1 Introduction

1.1 Challenges in Chemotherapy Development

Cancer is one of the leading causes of death worldwide, accounting for nearly 10 million deaths in 2020.[1] In Canada alone, over 1.5 million individuals have lived or are living with cancer, with over 230,000 new annual cases and 85,000 deaths in 2022. It is estimated that 43% of people will be diagnosed with cancer in their lifetime.[2] While incidence and death rates have slowly but steadily declined in recent decades, cancer remains a major concern with an aging and growing population.

Chemotherapy is extremely important in the treatment of cancer; in some instances, it is the primary treatment method, particularly with non-solid tumours like leukemia. However, in many instances, chemotherapy is an adjunctive treatment, used with or after surgery or radiation therapy, as patient relapse or metastasis is common.[3] Several factors go into deciding the therapeutic response to a tumour diagnosis. Tumour type is most obvious, as tumour cells have differing sensitivity, responsiveness, or resistance to various therapeutic agents. L-asparaginase, for example, is known to be effective against lymphocytic leukemias, depriving those cells of asparagine, which is essential to their function and survival.[4] Tumour location can pose specific challenges to treatment, such as the difficulty of delivering chemotherapeutic agents to a relatively avascular region, or across the blood-brain-barrier. High doses can systematically force drug to the desired site, but this also risks high systemic toxicity. Smaller tumours tend to be more responsive to treatment than larger tumours; many chemotherapeutic agents work on cells in active growth cycles, and smaller tumours tend to have a larger fraction of cells in this phase.[5] Smaller tumour burden also tends to correlate with healthier patient condition, which often means the patient is able to better tolerate the toxicity of the chemotherapy.

1.1.1 Tumour Growth

When we look at humans (and most other organisms on Earth) at a macro scale, bodies appear relatively static; however, when we zoom in, the body is constantly repairing and replenishing itself at the cellular level. Even without injury or illness, only a select type of cells, such as those associated with the central nervous system, will last a lifetime. Red blood cells tend to last around 4 months, epidermal skin cells might last anywhere from 10-30 days, and epithelial cells in the stomach and intestine rarely last a week.[6] Replacement of cells is carried out with a high degree of accuracy; in order to regulate normal cell growth and proliferation, the body uses growth factors, which are produced to communicate via specific cell receptors and stimulate them to undergo division. The presence of many different membrane receptors for different factors on a given cell suggest that multiple different growth factors are required to stimulate a cell to divide, which likely contributes to finer control and regulation of these functions.[7]

Cancer is a result of a breakdown of these normal control mechanisms. In most cases, damage to a cell simply results in its death. However, damage to DNA (often via chemicals, radiation, or viral infection) can sometimes cause mutations in specific genes known as oncogenes. These oncogenes are often responsible for some aspect of normal cell proliferation, including growth factors, growth factor receptors, and other enzymes involved with cell division.[8] Another type of gene involved are tumour suppression genes, which slow or stop cell growth/division, or trigger apoptosis (programmed cell death).[9] This lack of regulation due to mutations in these genes causes the affected cells to replicate uncontrollably, developing into a tumour mass. While some tumours are benign, malignant tumours will invade and destroy adjacent tissue, and clumps of these cells can break off into the lymphatic or circulatory system to form secondary, metastatic growths.[7]

1.1.2 Mechanisms of Chemotherapy

Chemotherapy agents encompass a wide range of compounds that affect tumour cells in different ways. They are generally grouped into a number of categories/classes depending on their chemical structure and/or mechanism of action. Some compounds have multiple mechanisms of action, and a single compound

may be classified under multiple different classes. Different types of agents are effective against different forms of cancer and tumour cells; even within a given type of agent, some drugs/compounds will be more effective than others at treating various malignancies.

Alkylating agents were one of the earliest studied groups of chemicals against tumour cells, and still remain a common choice for chemotherapy treatment.[10] Generally, alkylating agents damage DNA to cause lethal mutations via alkylation of DNA directly. While this is effective in inhibiting tumour growth, these agents are paradoxically potent carcinogens themselves, known to increase the risk of developing leukemia over the course of treatment.[11] Other types of agents also affect DNA directly including triazenes.[12]

Antimetabolites have very similar chemical structure to essential metabolites and combine with or are incorporated into nucleic acid or relevant proteins/enzymes. In doing so, they interfere with normal biological function by inhibiting their biological activity. This ultimately results in the breakdown of pathways essential to cell division and proliferation.[13] Antifolates specifically interfere and block with folate metabolism, which is essential in the biosynthesis of purine and pyrimidine for DNA. Anthracyclines are a class of antitumour antibiotic that do not cause direct mutations to DNA, but will bind to DNA, preventing its replication.[13]

1.1.3 Major Barriers in Chemotherapy

In general, treatment is limited by the negative effects a chemotherapeutic agent has on healthy cells. Tumour cells are practically identical to healthy cells, which means that the same mechanisms meant to affect and kill tumour cells and tissue also impact healthy tissue as well. One of the main reasons that cancers can be so dangerous also happens to be a major reason chemotherapy works as well as it does. Without proper regulating mechanisms, cancerous cells grow and multiply uncontrollably. Not only does this take up space and potentially damage surrounding tissue due to the tumour growth, but this constant proliferation is extremely resource intensive, so cancer cells will sap and consume resources at a much higher rate than normal healthy cells. Some solid tumours will even overexpress certain factors that promote

vascularization and angiogenesis.[7,14] This "behaviour" (so to speak) means that, in addition to up-taking a greater portion of nutrients, tumour tissue will also uptake a greater portion of chemotherapeutic agent, relative to healthy tissue.

However, healthy tissue will still inevitably be affected, and thus the body experiences toxic side effects of chemotherapy treatment. Some adverse effects due to chemotherapy toxicity include gastrointestinal distress, muscular weakness, alopecia, and loss of sensation. However, more severe side effects include cardiac damage, liver damage, and leukopenia/thrombocytopenia, which leaves patients vulnerable to infection or hemorrhaging, respectively.[15] The ratio of doses between therapeutic effect and toxicity is known as "therapeutic index".

The goal in development of chemotherapy technology is to increase the therapeutic index of both existing and novel treatments and agents. This can be done by increasing the therapeutic effect of an agent, and by decreasing its toxicity. Stronger chemotherapeutic agents have been in development to combat drug-resistant tumours that often lead to treatment failure or patient relapse;[3] they are designed to more aggressively eliminate a larger percentage of tumour cells. Unfortunately, many of these agents do not make it past clinical trials to market, as their increased effectiveness against tumour cells also corresponds with an increased toxicity to healthy cells, leading to more severe systemic toxicity.

In addition to toxicity, the development of new chemotherapy drugs is largely limited by bioavailability – the amount of drug in systemic circulation in the body; bioavailability affects the frequency and dosage required for a drug to reach therapeutic concentrations.[16] Hydrophobicity, degradation under physiological conditions or enzymatic processes, and rapid renal clearance are all factors that can negatively impact a drug's bioavailability and efficacy.

1.1.4 Mechanism of Curcumin

Curcumin (CUR), derived from the herb, *Curcuma longa* (commonly known as turmeric in the culinary world), has received a great deal of attention over the past few decades for its potential

biofunctional properties, particularly its anti-cancer potential. Several different mechanisms of action for its anticancer activity have been proposed and studied for CUR and its derivatives; it has been shown to interfere with several different cell signalling pathways including proliferation, apoptosis, the cell cycle and metastasis.[17,18] CUR has also been shown to assist in reducing multiple drug resistance in tumour tissue by downregulating P-glycoprotein expression.[19] These multiple pathway effects also make CUR a strong candidate for treatment of multiple types of cancers including breast, ovarian, gastrointestinal cancers, and even brain tumours due to its ability to pass the blood brain barrier.[17,20]

The safety and non-toxicity of CUR has been explored in several phase I clinical trials involving chemotherapy patients.[21–23] CUR was used in combination with another chemotherapy agents in these studies; minimal adverse side effects were noted. It has been suggested that CUR specifically impacts many pathways associated with oncogenic mutations, resulting in effective anticancer behaviour with lower adverse effects.[20] Many cancers affect the retinoblastoma (RB) pathway, which plays a key role in regulating the cell cycle and cell proliferation. These mutations typically affect proteins and enzymes involved in inhibiting cell cycle progression and DNA replication.[24] CUR increases negative regulator activity of the RB pathway, which suppresses phosphorylation of RB protein. Unphosphorylated RB protein prevents the cell from moving to the S phase of the cell cycle (DNA synthesis).[25]

CUR has also been shown to enhance effectiveness when used in conjunction with other anticancer agents. For example, CUR has been shown to upregulate the p53 signaling pathway, which is involved in pathogenesis and can induce cell apoptosis.[26] This has been shown to enhance anticancer activity of the chemotherapy agent, paclitaxel, in HPV-positive cancer cells via the p53 pathway.[27] These are by no means the only mechanisms of action for CUR; many other affected pathways have been studied and documented in the field of anti-cancer potential alone.[17,20] CUR has been shown to also have applications as an anti-bacterial or anti-inflammatory agent.[28–30]

However, despite proven efficacy via multiple mechanisms of action, it has not been adopted for use in clinical treatments. The biggest hurdle to this is its low bioavailability, which is a result of its

hydrophobicity, and rapid decomposition at neutral or alkaline pH, or exposure to light.[31] This has prompted research into micro- and nano-scale strategies to improve CUR solubility/stability and facilitate delivery *in vivo*. This project focuses on polymeric nanocarriers as a potential solution to CUR delivery.

1.2 Polymeric NPs

The field of nanotechnology encompasses a wide range of inventions, innovations and technologies designed at nanometer scales, typically no more than a few hundred nanometres (though some micrometer-scale technologies also tend to get lumped in, as they tend to be designed along similar purposes and principles). At the nanoscale, materials often behave much differently when compared to their "bulk" conditions, resulting in many emergent phenomena upon which these nanotechnologies are based. At nanoscales, the morphology of a material's surface can affect physical properties, such as the creation of "super non-wetting" surfaces that act similar to many waxy plant leaves, where water simply rolls right off, without necessarily requiring some hydrophobic surface coating (like wax, oil, or plastic).[32] We can also observe nanotechnology at the atomic structure level; carbon can have vastly different physiochemical properties depending on its structure. In its fully crystalline tetrahedral allotrope, it is diamond, one of the hardest substances, an electric insulator, and capable of transmitting and refracting light. On the other hand, graphene, the trigonal planar allotrope of carbon that forms a continuous hexagonal lattice, is extremely strong and flexible, as well as electrically conductive, but absorbs most wavelengths of light.[33]

In medicine, nanotechnology has been used in a variety of applications, from imaging organs, forming synthetic scaffolds for cellular growth/regeneration, to improving drug delivery. This project focuses on the latter. One of the most common ways to improve drug delivery is through nanocarriers. These can range from simply conjugating a drug to a molecule or nanoscale structure, to nanoparticles (NPs), and even drug loaded polymer matrices/scaffolds. NPs, which comprise a significant portion of nanomedicine solutions, can be made from a variety of materials. Metallic NPs are generally synthesized through nucleation and growth of metal formed by precipitation of elemental metal through the chemical reduction of metal salt.[34] Micelles and liposomes are formed by spontaneous assembly of amphiphilic molecules (often fatty acids)

in water, based on the dual hydrophilic and hydrophobic nature of the molecules' head and tail, respectively.[35] Polymeric NPs are formed when hydrophobic polymer dissolved in organic solvent is introduced to an aqueous solution, where it precipitates and forms NPs. Encapsulation of drug to enhance stability and solubility is most often done with the latter two types of NPs.

Nano and microscale structures and systems greatly expand the potential for drug delivery through several potential factors. Depending on the delivery system, they can assist in drug stability and circulatory half-life, enhance the viability of normally low bioavailable drugs, and/or facilitate targeted delivery and uptake.[36] As a result, these systems can increase therapeutic efficacy, reduce toxicological side effects, and improve patient compliance.[37] Polymeric NPs in particular have been explored as attractive nanoscale drug carriers. Encapsulation of drugs into these nanostructures improves stability and effective solubility, and polymeric NPs have been shown to be easily synthesized through both "bottom-up" methods (e.g., nanoprecipitation, salting out)[38,39] and "top-down" methods (e.g. solvent emulsion).[40]

1.2.1 PLGA

As a drug carrier, PLGA has been shown to successfully protect and transport a variety of agents, both hydrophobic and hydrophilic. It has been studied extensively for a variety of applications, including chemotherapy, but also vaccines, brain diseases, and even promoting bone regeneration.[41–43] PLGA is one of the few Food and Drug Administration (FDA) approved synthetic polymers due to biodegradability and biocompatibility. It degrades via hydrolysis into lactic acid and glycolic acid which are non-toxic. As a block co-polymer of poly-lactic acid (PLA) and poly-co-glycolic acid (PGA), its degradation properties can be controlled by modifying the ratio of PLA to PGA. The methyl groups present in lactic acid make the PLA block more hydrophobic than the PGA block, thus PLGA with a higher ratio of lactic acid to glycolic acid will generally degrade slower.[36,40,44] Degradation is also dependent on MW, with smaller, less polymerized PLGA degrading faster than larger MW polymer. The safety, control over degradation, and proven applications of PLGA make it a highly desirable nanocarrier material for this project as a model proof-of-concept NP core.

1.2.2 Chitosan

Additionally, the interest in natural polymers (chitosan, hyaluronic acid, cellulose, etc.) drug delivery nanomaterial candidates has grown, due to factors such as biocompatibility, biodegradability, inexpensiveness, and availability.[45–47] Specifically, chitosan has been investigated as a nanocarrier due to the amine groups along its backbone, which make it the only positively charged polysaccharide, and provide reliable points of conjugation for targeting moieties and other structural modifications.[48,49] A 2014 study showed that chitosan-coated NPs exhibited significant mucoadhesive properties compared to their uncoated counterparts; it is suggested that this property is related to the electrostatic forces between the cationic backbone and negatively charged groups within mucin proteins;[49] another study showed its potential to accumulate in tumour cells.[48] However, chitosan is limited by its low solubility in non-acidic environments, high viscosity in dilute aqueous acidic environments, limited drug release, and low encapsulation efficiency.[45,48,50]

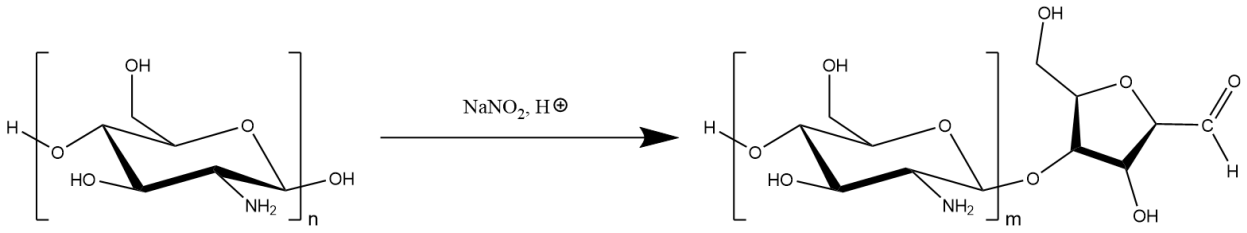

Figure 1-1: Nitrous acid depolymerization of chitosan, forming 2,5-anhydro-D-mannofuranose (amf) moiety, which contains a reactive aldehyde group.

Instead, chitooligosaccharides (COS), an oligomer of chitosan that can be prepared by depolymerization of chitosan with nitrous acid or hydrochloric acid, has been explored as an alternative that retains chitosan's desirable physical and chemical properties, while also having better solubility at pH closer to neutral.[50] Control over average oligomer length of COS in nitrous acid depolymerization has been shown to be controllable through the stoichiometric ratio between chitosan and nitrous acid.[50–52] This depolymerization also results in a reactive aldehyde group on one end of COS oligomers, which can be

functionalized with a variety of groups or moieties. A dihydrazide linker can be used to form a reactive amine site, as the hydrazide group is able to selectively react with the COS aldehyde; the hydrazide is generally more reactive than the other amine groups along the COS backbone (difference in reactivity can be further distinguished by adjusting pH, since the pKa of the hydrazide group is lower than that of primary amines).[53]

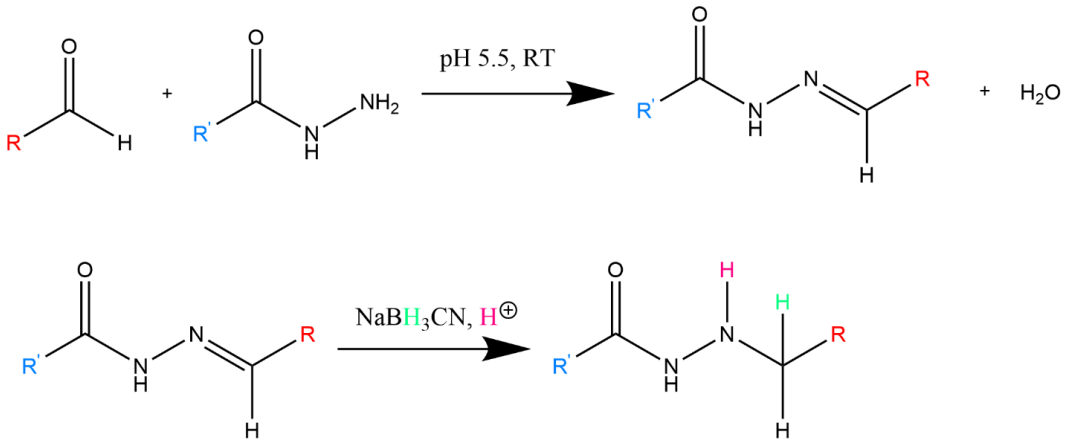

Figure 1-2: Reaction between hydrazide and aldehyde, which forms hydrazone conjugate. The hydrazone double bond is further reduced to a more stable secondary amine by $NaBH_3CN$.

The properties of synthetic polymers and natural polymers as nanomaterials compliment each other; the former provides tunability of drug release and simple nanostructure synthesis, while the latter provides customization of functional groups and targeting moieties for improved targeting and properties tailored to specific physiological environments. Recent studies have created hybrid nanostructures of synthetic and natural polymers, with synthetic polymers acting as the core structure and natural polymers acting as a coating, indirectly bound by adsorption and intermolecular forces.[47,49,54] Some studies have explored PLGA core, chitosan-coated NPs as potential drug nanocarriers.[54,55]

1.2.3 Integrins and Active Targeting

While chitosan has been shown to have potential for passive targeting of tumour cells, various ligands can be used in active targeting. Integrins are a family of receptors found in the extracellular matrix (ECM), and are mainly involved in cell-cell and cell-ECM adhesion interactions.[56] They are heterodimeric glycoprotein receptors that consist of noncovalently bound α and β subunits (hence their naming convention of α_β_ for classification).[57,58] Of these integrins, the $\alpha_v\beta_3$ integrin is among the most important in tumour angiogenesis, and is overexpressed in several tumour types including ovarian and breast cancers.[59] In normal tissue, $\alpha_v\beta_3$ integrin plays a key role in endothelial cell survival and the migration process during angiogenesis, and is only expressed in response to angiogenic growth factors. It is found expressed at wound sites or site of inflammation. Biopsied tissue shows that this integrin is highly expressed in tumour blood vessels, but not normal, healthy blood vessels.[57] The $\alpha_v\beta_3$ integrin serves as a receptor to many ECM molecules that contain the Arg-Gly-Asp (RGD) peptide sequence; as such, ligands based on the RGD peptide, as well as RGD mimetics, have been shown to deliver targeted therapeutic doses of anticancer drugs like Paclitaxel and Doxorubicin to tumour cells.[56,60–62] The presence of -COOH carboxyl groups in RGD peptide allows for conjugation to COS via NHS-amine reactive chemistry. This allows COS-coated PLGA-core NPs to be functionalized with RGD peptide for active targeting and drug delivery.

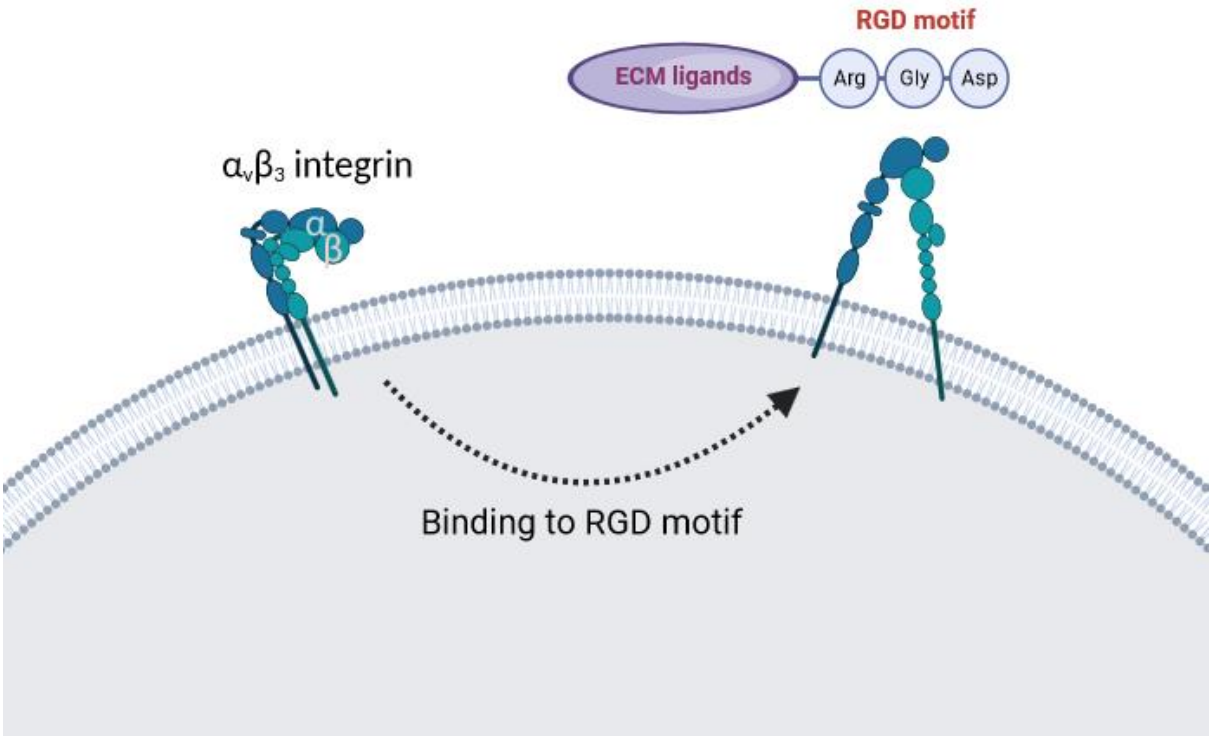

Figure 1-3: Illustration of the $\alpha_v\beta_3$ integrin, a heterodimer, which binds to a variety of ECM ligands through affinity with the RGD peptide motif. Created with Biorender.com.

1.3 Techniques in NP Synthesis

1.3.1 NP Synthesis Methods

There are a variety of methods to produce various nanocarrier systems, including direct conjugation of drugs to PLGA molecules, drug-loaded scaffolds, and drug-encapsulated NPs; this project focuses on the latter system, for its ability to travel systemically to the tumour site, and for the protection of the drug from physiological conditions.[41,42] It is important that the method of synthesis be relatively facile, occur under "mild" conditions (temperature and pressure close to standard conditions, minimal use of volatile, toxic compounds), and require minimal complex equipment. As a proof-of-concept with a limited time-frame, throughput is important (in addition to the obviously essential quality and replicability of the NP product). This means that, while spray drying may be more suitable for scalable production, the upfront

cost of a spray dryer would likely not be worth the investment if an alternative synthesis method could provide similar NP quality.[63]

Based on these requirements, there are 2 synthesis methods to consider: emulsion method and nanoprecipitation. The emulsion method is generally the simplest and most straightforward, consisting of the formation of an oil-in-water emulsion between water and PLGA with the drug dissolved in an immiscible organic solvent (like DCM) in the presence of an emulsifier/surfactant like PVA or vitamin E-TPGS, often by sonication.[40] The mixture is allowed to stir so that the organic solvent can evaporate, leaving "hardened" PLGA NPs suspended in an aqueous solution. NPs can then be washed, purified, and freeze dried for storage/future use. In the case of hydrophilic drug where it cannot dissolve into the organic phase, the double emulsion method can be used. This is essentially identical to the single emulsion method, except that the drug is introduced into the organic phase by first creating a water-in-oil emulsion. This primary emulsion is then once again emulsified to create a water-in-oil-in-water emulsion.[40]

Nanoprecipitation also involves the mixing of PLGA and hydrophobic drug dissolved in an organic solvent into a large volume of water or aqueous buffer often containing surfactant. However, in the case of nanoprecipitation, the organic solvent is miscible in water. This organic mixture containing PLGA and the hydrophobic drug is slowly added to the aqueous medium, causing the polymer and drug to precipitate out of solution, forming NPs. These NPs are stabilized by the presence of surfactant and evaporation of the organic solvent from solution.[38,64]

While the two methods are both relatively replicable, the emulsion method was ultimately chosen for its throughput, given equipment present in the lab. To maximize replicability, addition of organic phase for nanoprecipitation would need to be performed with a syringe pump; with the emulsion method, having an automated tip sonicator would allow similar replicability by controlling sonication amplitude, pulse time and duration. Addition of organic solvent with the pump system could take several minutes (especially depending on volume), while sonication could be done in approximately 1-2 mins, regardless of volume (within reasonably small scales, which was not an issue during preliminary testing). Cleaning the sonicator

between samples would also be much less time consuming than cleaning the syringe pump. Lastly, evaporation of most miscible organic solvents used in nanoprecipitation like ethyl acetate is generally noticeably slower than evaporation of immiscible volatile solvents used in emulsion method like DCM. While a multi-position stirrer was available to handle the stirring of multiple samples, it was not feasible to set up a negative pressure system to facilitate quicker evaporation. Replicability of NP size and PDI was shown to be adequate in preliminary synthesis of void PLGA NPs (which is evident in the NP size and PDI data shown later).

To isolate and purify the NPs, they can be put through a series of centrifugation and wash cycles with an aqueous buffer. High centrifugation speeds suggest that the NPs harden and stabilize successfully, resisting irreversible aggregation even under those increased forces.[42,55,65] For long-term storage of PLGA NPs, it is important to dry it into a powder, as the PLGA and drug are still susceptible to hydrolytic degradation in aqueous suspension, or even from latent moisture. Lyophilization, also known as freeze drying, is a relatively well-established and common process to remove water and improve NP stability. In brief, lyophilization bypasses the liquid phase of water entirely by cooling the solution beyond its triple point, then allowing it to heat up under negative pressure (vacuum). Instead of melting and evaporation, the ice within the material experiences sublimation, which generally maintains material structure far better than conventional processes. It is a gentle water removal process, in contrast to conventional evaporation, which relies on heating the product.[66] Both the heat and evaporation of water itself can damage and degrade the structure of the NP, and the drug encapsulated within. However, the lyophilization process can still negatively affect the physical stability of NPs, particularly by the formation of ice crystals, and potential aggregation during sublimation. Cryoprotectants, often a sugar like trehalose, mannitol, dextran, or sucrose, have been used to reduce overall aggregation and improve stability throughout the lyophilization process.[67–69] One theory for this behaviour is the "water replacement theory", which generally hypothesizes that the removal of water molecules between NPs causes aggregation/instability, and that the cryoprotectant acts to maintain the separation of NPs even as the water is removed via sublimation.[66] The mechanism that allows

these cryoprotectants to mitigate NP instability at the freezing stage is less well-understood -- however, studies of freezing and thawing cycles with PLGA NPs and various sugar cryoprotectants showed that glucose, sucrose and trehalose were successful at maintaining NP size distribution at concentrations as low as 5% (w/v).[67]

1.3.2 Chemical Conjugation

The two most common methods of coating polymeric NPs are physical adsorption and direct chemical conjugation. When coating synthetic polymeric NPs with another synthetic polymer, it is common to use chemical means to simply form a di-block co-polymer of the two polymers; this tends to result in a core-shell type of polymeric nanocapsule or micelle-like structure, with the more hydrophobic polymer serving as the inner core, and the hydrophilic polymer serving as the outer shell. Polylactic acid (PLA), PLGA, and poly-ε-caprolactone (PCL) have been explored as "core" materials, while polyethylene glycol (PEG), tocopherol polyethylene glycol succinate (TPGS), and polyethylenimine (PEI) have been used as outer "shell" materials, for anti-cancer delivery applications.[65,70–75] This is by no means an exhaustive list and simply describes some of the more common and recurring polymers used in anti-cancer NP delivery.

Many natural polymer coatings do not involve covalent chemical bonding, and instead rely on physical adsorption to the NP surface. Several different polysaccharides have been explored as NP coatings, including chitosan, hyaluronic acid, tannic acid, alginate, and dextran.[55,76–80] While some of these natural polymers are coated after NP formation, several projects have explored using these polymers as the emulsifiers themselves to stabilize NP during emulsion assembly. Chitosan's positively charged functional groups makes it uniquely able to adsorb to the surface of NP formed from negatively charged synthetic polymers (i.e. the carboxyl groups on PLGA) via electrostatic interaction. The proposed mechanism of adsorption for other natural polymers seems to be hydrogen bonding via -OH or -NH groups along their backbones.

Reliance on physical adsorption for coating of natural polymers may result in decreased stability and sensitivity to changes in pH, ions, temperature, and/or solvents. In contrast, chemical conjugation via forms of covalent linker chemistry can be more resilient, as well as less reliant on physical and electrostatic compatibility of polymer moieties. Amine-reactive crosslinker chemistry can allow for relatively straightforward and facile chemical conjugation because the reaction is regioselective and occurs under benign conditions (aqueous, room temperature, moderate pH).[81] NHS ester groups, which can be created by modifying carboxyl groups with EDC (N-(3-Dimethylaminopropyl)-N'-ethylcarbodiimide hydrochloride) and stabilized with NHS (N-hydroxysuccinimide), are often used as an amine-specific functional group for linking or labelling.[82] EDC reacts with carboxyl groups to form an unstable, highly reactive o-Acylisourea intermediate, which can form an amide bonded conjugate if in the presence of an amine group, but can also revert back to a carboxyl group via hydrolysis.[81] NHS can create a semi-stable NHS-ester, which is still reactive to amine groups. The EDC-carboxyl reaction occurs optimally between pH 4-6; in addition to an incompatibility with carboxylate and amine buffers, EDC also reacts with phosphate groups.[83] The NHS-ester amine reaction, however, prefers slightly alkaline conditions (pH 7-9), as the amine reaction must also compete with the hydrolysis of the NHS-ester back to a carboxyl.[81,82] Though the carboxyl conversion to NHS-ester can be prepared in advance, separate from the NHS-ester amine reaction, this conjugation has been successfully performed in a single reaction vessel, at pH around 5.[50,52] Excess EDC and NHS are used, such that any incomplete reversion of carboxyl group from either o-Acylisourea or NHS-ester via hydrolysis would have more EDC/NHS reagent to react with again.

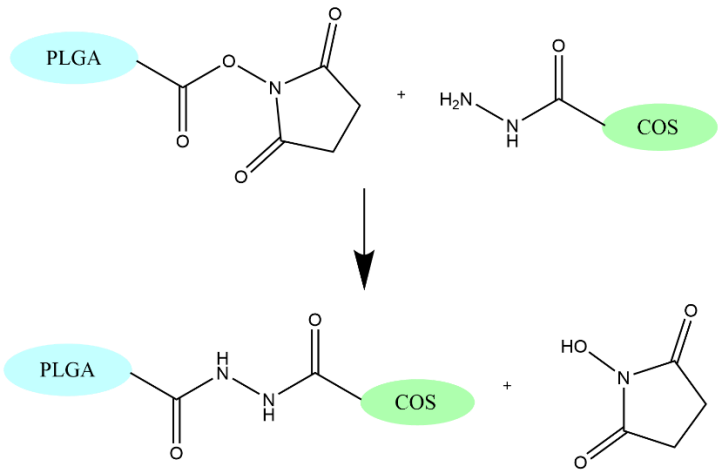

Figure 1-4: Secondary amide formation between NHS and hydrazide group, which links COS to PLGA. This reaction occurs under acidic conditions (pH 4-5).

Another method of direct covalent chemical conjugation is using click chemistry, which generally refer to a group of "click" reactions that occur with high product yield and under benign conditions – they do not need significantly elevated temperatures, and are mostly insensitive to the presence of water or oxygen. Most click reactions can also be purified without the need for chromatographic separation.[84] Click reactions are highly selective, hence the name, referring to the way specific puzzle or Lego pieces might "click" together easily. One of the most common click reactions is the Cu(I)-catalysed azide/alkyne cycloadditon (CuAAC), which, as its name states, involves the copper catalyzed reaction between azide and alkyne groups to form a cyclic triazole linkage.[50] One major drawback of this reaction to the project is that copper has a strong affinity for chitosan, which would make removal of copper from the NP system extremely difficult. One alternative to CuAAC that has been explored is eliminating the copper catalyst by using a cycloalkyne instead of a linear alkyne end group. This takes advantage of the angle strain inherent in these cyclic structures to help facilitate the click reaction which is known as strain-promoted azide/alkyne cycloadditon (SPAAC).[85,86] One of the most common candidates for this reaction is the dibenzocyclooctyne group.

Chemical conjugation of polymeric NPs can occur before or after NP formation. Each option has their respective advantages, disadvantages, and limitations. Conjugation before NP formation can be the most straightforward process; the core NP material and coating material are dissolved in solution with any necessary binding reagents, catalysts, etc., and reacted for a requisite amount of time before the reaction is stopped, and the product is isolated and purified. Conjugation after NP formation involves adding the coating material to the suspension of NPs and performing the reaction at the NP surface. Excess reagents would then be removed to purify the NPs. With the former method, the process is usually quite facile, and in some cases, conjugation of the coating molecule directly to the core NP molecule to form a "two-domain system" before NP formation can be actively beneficial to the formation process. In the case of differing hydrophobicity, if the coating material is more hydrophilic, this can aid in the formation of the NP, as the more hydrophilic domain interacts strongly with the aqueous continuous phase, while the more hydrophobic domain (which will be the core of the NP) can interact with the dispersed organic phase during NP assembly. The presence of certain functional groups on the coating molecule could also provide electrostatic or steric hinderance to improve general NP stability without the need for more surfactants, emulsifiers, or other stabilizers. This method does suffer two major drawbacks, however. The first is issues of mutual solubility between both the core NP molecule and coating molecule; if conditions cannot be found that enable both molecules to be solubilized simultaneously (or the conditions required are unsuitable for the necessary linking reaction), yield for the reaction will be extremely low. Secondly, if the core NP molecule contains multiple binding/reaction sites, some of the binding configurations could be poorly suited or incompatible with the assembly of the NP structure (i.e., if binding occurred along the polymer chain instead of one of the end groups).

In contrast, performing conjugation of the coating molecules onto formed NPs requires consideration for the state and stability of the NPs. The surface charge (zeta potential) is important in maintaining colloidal NP stability via electrostatic interactions; this can be affected by changes in pH of the medium.[87–90] Many reactions require a certain range of pH values to be efficient/effective, which may be outside the pH range

that would maintain NP stability. The main advantages of conjugation after NP formation is that you do not have to work around differences in solubility between NP and coating, and you do not have to work around regioselectivity with respect to the NP polymer molecule. So long as the NPs remain suspended and stable, the only interface available for reaction is at the NP surface. This provides a high surface area for reaction that would not be available if the core NP material was insoluble on the bulk scale, and that the coating material will only end up reacting with the surface.

1.3.3 Characterization

After each major step, the NPs (and related materials) should be characterized to ensure successful synthesis, as well as to track quality and consistency. Nuclear magnetic resonance (NMR) spectroscopy is a spectroscopic technique that takes advantage of the magnetic properties of certain nuclei to identify specific molecular structures. The sample is placed under an external magnetic field and irradiated with pulses of electromagnetic radiation; energy is re-emitted by the sample, which is collected as data and then translated into a spectral graph via software.[91] In ^{1}H NMR (aka proton NMR) specifically, the ^{1}H-atoms present in a given molecule resonate at specific frequencies determined by the chemical structure of the molecule, and their place in that structure. This allows for the determination of the presence of various molecular structures, from amines to carboxyl groups, and even distinguish between single bond and double bond carbon chains. NMR data also distinguishes the relative number of ^{1}H atoms of a particular chemical structure, which can be useful in determining the number of functional groups in a molecule, or units in a polymer chain.[92] NMR analysis of COS can determine the average size of the oligomers, and detect the presence of relevant chemical groups/structures; the aldehyde group should be present after depolymerization, but absent after reaction with the dihydrazide. The alkyl chain present between the two hydrazide groups is not found in COS, and thus should show up during successful reaction as well.

Fourier transform infrared (FTIR) spectroscopy is a similar spectroscopic technique that determines chemical structure from the specific infrared radiation absorbed by different bonds in the molecule. One major advantage of FTIR over NMR is that NMR requires the sample be fully solubilized in deuterated solvent, while FTIR can be performed on samples as dry powder.[93] However, the differences in FTIR spectra between chitosan and COS may be difficult to identify, as FTIR does not provide relative numbers of each atom/bond. Thus, it may be contingent on whether FTIR of the two materials can resolve a single specific bond, such as the C=O aldehyde.

Though NMR can give the number-average size of a polymer, it is unable to determine the size distribution. Matrix-assisted laser desorption/ionization coupled time-of-flight (MALDI-TOF) mass spectrometry (MS) is able to determine the mass of individual molecules, and thus the size distribution of COS produced through depolymerization technique. Samples dispersed in a suitable matrix are essentially vaporized and ionized by laser; these ionized particles are then accelerated via electric field, which filters and separates the molecules based on their mass-to-charge ratio.[93] The TOF spectrometer works by pulsing "shots" of ionized sample, as lighter ions with higher charge will reach higher speeds faster than heaver molecules with lower charge, thus reaching the detector faster or slower. One major issue in this case is that chitosan is formed by the N-deacetylation of naturally occurring chitin.[94] Most commercially available chitosan is not fully de-acetylated, which means that some monomer units will be acetylated, while other will not. This will result in variance across polymer/oligomer MWs, even those with the same number of units, which will in turn cause issues for accurately determining size distribution.

Dynamic light scattering (DLS) is a technique to determine the size and distribution of suspended NPs, by analysing fluctuations in light scattering of these particles caused by their Brownian motion.[95] It is one of the most common and facile methods to determine NP size distribution; samples do not require special preparation, and modern DLS systems can typically automate much of the optical optimization. A similar technique is electrophoretic light scattering (ELS), which is based on DLS, but measures fluctuations in scattering from particles experiencing motion due to an oscillating electric field. As this motion is

dependent on the charge of the particle, ELS is able to determine the surface charge, or zeta potential, of particles in suspension.[96] NP size and monodispersity is important to control behaviour of the NPs such as permeability and uptake through membranes, but large NP size and polydispersity can also signal aggregation, which is a telling sign of poor NP stability. Zeta potential is also important for determining NP stability, as electrostatic interactions are often a major factor in keeping NPs from aggregating with each other.[90] However, zeta potential can also be important in determining whether NP coatings are successful, and zeta potential plays a major factor in determining how well NPs are adsorbed onto cell membranes.[87,89]

Ultra performance liquid chromatography (UPLC) is a chromatographic technique to separate and analyse various analytes dissolved within a given sample. The sample is flowed through a special porous column at extremely high pressure using a "mobile phase" (typically a specific mixture of organic solvent and aqueous buffer); Different analytes will interact and adsorb to the column material (called the "stationary phase") to varying degrees, typically based on the polarity of the analyte, which affects how fast each analyte elutes through the column.[97] As the sample is flowed through, different analytes are separated by how long it takes to elute, and can be analysed by UV-Vis or fluorescence detectors. UPLC avoids the issue of needing to separate or purify multiple analytes, or even one specific analyte from the rest of the sample (i.e., to measure CUR drug encapsulated within PLGA NPs in solution). UPLC is more sensitive and efficient than traditional UV-Vis spectroscopy, and even high-performance liquid chromatography (HPLC); the small column diameter and high pressure result in faster elution times, with less sample required, and typically a better sensitivity for detection of analytes at low concentrations. To obtain optimal separation and elution of analytes, it is important to optimize parameters including the composition of the mobile phase (most importantly the ratio of organic to aqueous medium) and overall flowrate. The process of optimization is generally a balancing act between mobile phase composition and flowrate, as both factors affect and are limited by system backpressure. Organic solvents are typically lower in viscosity and thus more organic solvent in mobile phase decreases the system backpressure; higher

flowrate results in higher backpressure. Lower organic composition mobile phase will typically result in larger separation between analyte elution times, but the increase in backpressure limits the achievable flowrate, which can prolong the analysis time of samples significantly. Thankfully, many UPLC systems allow for the automation of gradient mobile phase flows, meaning that the composition and flowrate of the mobile phase can be gradually adjusted throughout a sample's analysis (or "runtime"). This may be highly important in successfully separating CUR from metabolites or derivatives during analysis.

1.3.4 Assays for Characterization

Assays are essential in determining the success at various steps of the project. Assays use specific chemical reactions to selectively determine the presence of specific functional groups, or even types of molecules (e.g. proteins), known as the analyte. While some assays can only provide a qualitative assessment on whether the analyte was detected, many assays provide measurable, quantitative results about the analyte. Most assays make use of colorimetric or chromogenic "dyes" as reagents to measure analyte activity and can be analysed in a UV-Vis spectrometer at wavelengths specific to each dye. A convenient and effective way to perform assays at higher throughputs is the use of a UV-Vis spectrometer microplate reader.

With some assays, the dye molecule may interact directly, changing form or forming complexes with the analyte which causes the colorimetric change, like with the Biuret reaction, an early test for protein determination that relied on the complex formation of cupric ions from copper sulfate with proteins in a strongly alkaline solution. This results in a purple-violet colour produced. Other assays rely on indirect interactions between analyte and dye, such as with the bicinchoninic acid (BCA) assay, which also uses the reduction of cupric ions; however, BCA complexes with the reduced Cu^{1+} ions, forming a purple complex. While the latter assay is more sensitive, there is a wider range of non-analyte molecules that can interact and interfere with both the copper reduction reaction and the BCA reagent of the BCA assay, than just the copper reduction present in Biuret reaction.[98] One factor that stands out as beneficially important in favour of using BCA assay for this project is that, because it detects protein/peptide concentration indirectly

through complexing with the generated Cu^{1+} ions, the BCA assay is still relatively accurate when dealing with proteins that are adsorbed or attached to a surface.[99] Thus, it would be able to quantitate the amount of RGD peptide free in solution, but also the RGD peptide conjugated directly to the NP surface.

However, it is important to consider restrictions and incompatibilities with different assays. Assays are not perfectly selective, and certain reagents or buffers may react with assay reagents, interfering with results; for example, the BCA assay is sensitive to NHS, which means the sample preparation or experimental protocol must be adjusted accordingly.[100] In most cases, proper washing/purification of NPs can remove NHS past the limit of detection. However, in some samples (such as monitoring the supernatant during the conjugation of RGD peptide to NP surface), it will not be feasible to remove NHS; instead, NHS concentration in sample can be controlled and accounted for by ensuring samples and standard curve all have the same NHS concentration. Another limitation of some assays is sensitivity. 2,4,6-trinitrobenzene sulfonic acid (TNBS) assay reacts with primary amines, making it a potential candidate for an effective assay to detect the presence of COS (primary amine backbone).[101] Unfortunately, preliminary experiments with TNBS assay on COS showed that the assay did not meet the desired limits of detection at the desired concentrations.

It is important in the assessment of drugs and treatments to determine its toxicity, and how the treatment group might negatively affect cells (in the case of anticancer agents, this is a feature, and not just an adverse effect). When determining cytotoxicity, a common way to measure how many cells die during treatment is to instead measure how many cells live through the treatment. Cell viability assays measure cell activity by using reagents that can measure some aspect of metabolic or enzymatic activity within cells. The methods for determining cell viability include tetrazolium reduction, resazurin reduction, protease markers, and ATP detection.[102]

3-(4,5-dimethylthiazol-2-yl)-2,5-diphenyltetrazolium bromide (MTT) and 3-(4,5-dimethylthiazol-2-yl)-5-(3-carboxymethoxyphenyl)-2-(4-sulfophenyl)-2H-tetrazolium (MTS) are tetrazolium salts that both form coloured formazan products when reduced by NAD(P)H-dependent oxidoreductase enzymes.[103,104]

This reaction occurs within active mitochondria of cells; when the cells die, they lose their ability to convert tetrazolium to formazan. The main difference between the MTT and MTS assays is that the formazan product produced by MTT is an insoluble precipitate, which must be solubilized before recording its absorbance. Solubilization is done with some combination of organic solvent (DMSO, ethanol, etc.), detergent (like sodium dodecyl sulfate, aka SDS), and acidification. MTS, on the other hand, generates a formazan product that is directly soluble in cell culture medium, but also requires an electron acceptor intermediate such as phenazine methyl sulfate (PMS) or phenazine ethyl sulfate (PES); the intermediate is reduced in the cytoplasm, where it exits the cell and converts MTS to soluble formazan.[105] These intermediates are necessary because the negatively charged portion of the MTS molecule that contributes to the aqueous solubility of formazan product also limits the cell permeability of MTS. The main advantage of the MTS assay is that MTS and PMS/PES can be mixed into a single solution, resulting in a one-step incubation, whereas MTT assay requires a second solubilization step, as solubilization agents would also result in cell death.

Resazurin, a non-fluorescent blue substance, can be metabolized by active, viable cells to form a pink and fluorescent resorufin product.[106,107] The main advantage of resazurin is the fluorescence of the metabolized resorufin; fluorescence measurement is more sensitive than absorbance measurement. It may be less susceptible to interference from non-fluorescent compounds, but more susceptible to other fluorescent compounds. In general, resazurin reduction assays have been shown to be slightly more sensitive than tetrazolium reduction assays. One significant drawback is that resorufin has been shown to be further reduced to a non-fluorescent product by active cells. Thus, under certain conditions, a treatment group containing highly viable cells may appear to yield low fluorescent signal, whereas a treatment group containing dying cells could yield a higher signal, as they would not sustain further reduction.[107]

Glycylphenylalanyl-aminofluorocoumarin (GF-AFC) uses protease activity to detect cell viability. GF-AFC is converted to aminofluorocoumarin (AFC) by aminopeptidase present in live cells' cytoplasms. In dead cells, this protease activity disappears rapidly, thus the generation of AFC is proportional to the

amount of living cells only.[108] AFC is able to generate a fluorescent signal to determine the relative cell viability of a sample. The main advantage of this protease activity assay over resazurin and tetrazolium reduction assays is that the latter two are toxic to cells, whereas the former is relatively non-toxic.[102] This can allow for multiple cytotoxicity evaluations on the same sample.

Measuring ATP is also a commonly applied method of estimating the amount of viable cells; as cells die, they stop synthesizing ATP, and ATPases rapidly deplete remaining ATP in the cell's cytoplasm. Unlike the previous methods which required incubation time for metabolic/enzymatic processes to transform the reagents into their coloured products, ATP assays immediately lyse the cells and measure ATP using firefly luciferase. Incubation times of tetrazolium, resazurin and protease activity assays vary from 1-4 hours, while ATP assays reach steady-state within 10 mins. ATP assays also eliminate variance from plate handling steps involved in incubation of the cells.

1.4 Rationale and Hypothesis

The main goal of this study was to develop a modular nanocarrier system utilising facile assembly and conjugation methods that could be used with interchangeable core and coating materials, to accelerate successful development of chemotherapy agents. NPs were assembled through the commonly used emulsion method, with PLGA as the core material, and CUR as the encapsulated model drug. These NPs were coated with COS and RGD in tandem to promote targeting of cancer cells. Physical properties of coated NPs were compared to bare PLGA NPs, and the formulations were compared *in vitro* via fluorescent cell uptake study and cytotoxicity assay with OVCAR-3 human ovarian tumour cells.

This project hypothesizes that PLGA NPs will successfully encapsulate CUR to protect from degradation and provide prolonged release, and that NPs coated with COS and RGD will provide better uptake and cytotoxic effects compared to bare PLGA NPs.

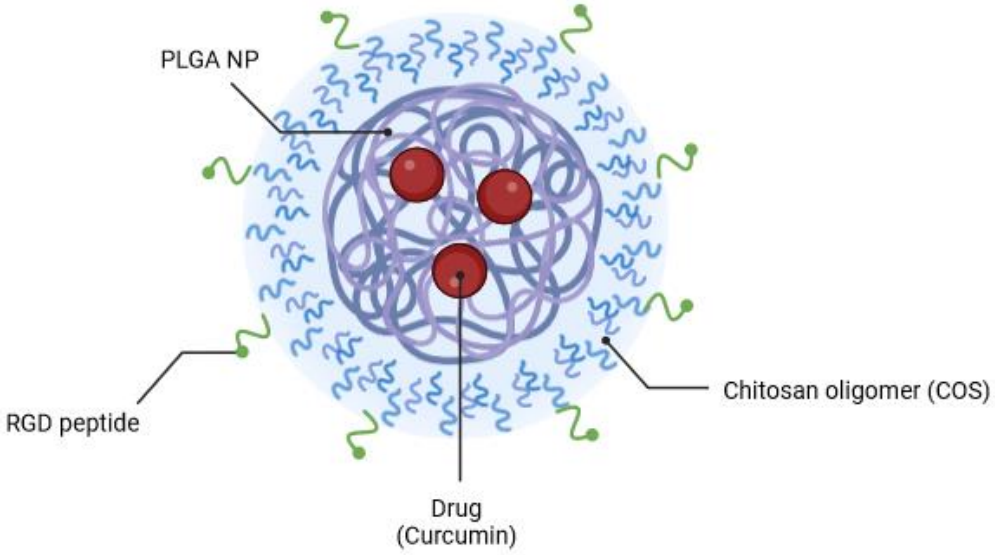

Figure 1-5: Illustration of the PLGA-COS-RGD NP encapsulating CUR drug. Created in Biorender.com.

1.4.1 Objectives

Objective 1: synthesize COS from chitosan via depolymerization, functionalize with reactive hydrazide group.

Objective 2: synthesize PLGA NPs loaded with CUR drug via emulsion method, conjugate NP surface with COS, RGD peptide.

Objective 3: Characterize drug-loaded NPs (size, coating, drug encapsulation, drug stability, cell uptake and viability).

2 Methodology

2.1 Materials

Adipic acid dihydrazide, ammonium hydroxide solution (28.0-30% NH_3 basis), ammonium acetate, chitosan (low molecular weight), curcumin (≥94% (curcuminoid content), ≥80% (Curcumin)), dimethyl sulfoxide (DMSO), glacial acetic acid, hydrochloric acid (37%) (HCl), MES (4-Morpholineethanesulfonic acid), methanol, methylene chloride (DCM), N-(3-Dimethylaminopropyl)-N′-ethylcarbodiimide hydrochloride (EDC), N-Hydroxysuccinimide (NHS), poly(vinyl alcohol) (MW 30-50K, 98-99% hydrolyzed/87-90% hydrolyzed), RGD peptide (Arg-Gly-Asp), sodium cyanoborohydride ($NaBH_3CN$), sodium nitrite ($NaNO_2$), trehalose dihydrate were all purchased from Sigma Aldrich. PLGA-COOH (poly (lactic-co-glycolic) acid) (50:50, 40K MW) was purchased from Nanosoft Polymers. Cytiva HyClone™ RPMI 1640 Media with Glutamine, Gibco™ Fetal Bovine Serum (certified, heat inactivated), Gibco™ Penicillin-Streptomycin, Phosphate-buffered saline (PBS, 1X, pH 7.4), Pierce Micro BCA Protein Assay kit, Promega CellTiter 96™ AQueous One Solution Cell Proliferation Assay (MTS) were purchased from Thermo Fisher.

2.2 Equipment Methods

Tip sonication of NP samples were performed with QSonica Q125 Sonicator. Samples were sonicated at 60% amplitude, at 15 s ON, 5 s OFF pulse, for 90 s. Tip was moved around in sample solution during initial sonication pulse to ensure all the organic portion was fully emulsified. Particle size/distribution and zeta potential of NPs were measured by DLS and ELS using Malvern Zetasizer Ultra-Red.

^1H NMR spectroscopy was performed on Bruker 500 MHz spectrometer at 300 K. All samples were dissolved to approximately 10 mg/mL in appropriate deuterated solvent (D_2O, acetonitrile-d3, dimethyl sulfoxide-d6). To facilitate the dissolution of chitosan-containing samples, pH of samples were decreased by adding 0.5% v/v HCl (12 M). NMR spectra was analysed using Bruker TopSpin NMR data analysis software.

Colourimetric assays were recorded and analysed using Varioskan LUX 3020 Multimode Microplate Reader. Coumarin-6 dye experiments were also quantified using plate reader. Assays were prepared in clear bottom 96-well plates. Well volume varied from 100 to 300 µL. Analysis of CUR content was performed using UPLC, using Waters Acquity UPLC H-Class Plus system. The column used was Waters ACQUITY UPLC HSS C18 Column (100Å, 1.8 µm, 2.1 mm x 100 mm; pore size, diameter, dimensions). Mobile phases were as follows: phase A – acetonitrile (ACN) (100%); phase B – 10% acetonitrile, 90% 10 mM o-phosphoric acid aqueous buffer. For sample analysis, flow parameters of each run were kept at constant flow rate of 0.4 mL/min, with gradient mobile phase composition. Percentage composition is given as XX% (by volume) mobile phase A; the remaining mobile phase is composed of mobile phase B. From 0-0.5 min, 44.4% A. From 0.5-1.0 min, gradient increases from 44.4% to 77.7% A. This gradient is held until 3.5 min. From 3.5-4 min, gradient is decreased back to 44.4% A, and held for the rest of the run. This results in a 50/50 ACN/water ratio to start and end, with a gradient to 80/20 ratio in between. PDA (photodiode array) UV-Vis absorbance detector was set at 430 nm.

2.3 Functional Chitooligosaccharide Synthesis

COS was prepared from chitosan through nitrous acid depolymerization based on the protocols by Moussa [50,52]; low MW chitosan was dissolved in 0.15 M HCl (2 g chitosan per 100 mL solution), then vacuum degassed to remove oxygen from the solution. 500 mM $NaNO_2$ aqueous solution was prepared (with degassed MilliQ water, immediately before addition to chitosan solution), which was then added for a GlcN:$NaNO_2$ molar ratio of 10:1 (to achieve COS with approximately 20 average GlcN units), before being stirred moderately overnight so as not to introduce excess oxygen to the mixture. The mixture was filtered to remove undissolved chitosan and other impurities, before precipitating COS by addition of ammonium hydroxide until reaching solution pH 9. To further increase yield, an equal volume of methanol was added to the mixture, which was then centrifuged for 10 mins at 10,000g and 4C. The COS was washed

(x3) by repeated centrifugation in 50/50 water/methanol, before a final wash step with water. The COS was then resuspended in 10 mL water and lyophilized.

Hydrazide functionalized COS (COS-hydrazide) was prepared by dissolving COS in water, with additions of acetic acid. MES was then added to a concentration of 0.15 M, before adjusting the solution to pH 4.5 with HCl or NaOH. 10 molar equivalents (to COS) of adipic dihydrazide was added to solution and stirred at RT for 24 h, then 10 molar equivalents (to COS) of sodium cyanoborohydride was added to solution and stirred at RT for 24 h. The COS-hydrazide solution was filtered, precipitated, washed and lyophilized following the same protocol as COS.

COS and COS-hydrazide were analysed with H NMR spectroscopy to confirm average size and presence of aldehyde or hydrazide groups, respectively. 5 μL HCl (12 M) was added to H NMR COS samples to facilitate dissolution in D_2O. COS was also analysed with MALDI-TOF MS to attempt to determine size distribution.

2.4 Synthesis of PLGA-COS NPs

Void (without encapsulated drug) PLGA NPs were prepared by emulsion method, based loosely on the works of Rafiei and McCall [40,109]. The initial emulsion mixture consisted of 1:4 v/v organic to aqueous parts. The organic portion was PLGA (acid-terminated) dissolved in DCM to a concentration of 50 mg/mL, while the aqueous portion was 3% w/v PVA. The mixture was briefly vortexed, then emulsified under ice bath. The emulsified mixture was then diluted with 1% PVA solution to 300% of its original volume and stirred for 3 h to evaporate the organic solvent. The NP mixture was centrifuged (15,000g, 10 min, 4°C) and washed with water (x3) to remove excess PVA, before being resuspended in 5 mL DI water (and 5% w/v trehalose as cryoprotectant if necessary) and frozen for lyophilization. A small aliquot was reserved for measuring NP size and ZP.

PLGA-COS NPs were formed by chemically conjugating COS-hydrazide to the surface of PLGA NPs using amine-reactive NHS chemistry. COS-hydrazide was dissolved in a small amount of dilute HCl before

being added to MES buffer (100 mM, pH 5) to a COS concentration of 5 mg/mL. PLGA NPs were added resuspended in this solution (2:1 PLGA:COS w/w), along with NHS and EDC (approx. 20%, 30% w/w PLGA NPs, respectively). The mixture was stirred vigorously overnight before washing excess NHS, EDC and COS through centrifugation. A small aliquot was reserved for measuring NP size and ZP, while the rest was prepared for lyophilization as previously described with PLGA NPs.

2.5 Synthesis of PLGA-COS-RGD NPs

RGD peptide was chemically conjugated to COS amine groups through amine-reactive NHS chemistry. 1 mg RGD peptide was added to 10 mL MES buffer (100 mM, pH 6.5) along with 0.5 mg NHS, 2 mg EDC. PLGA-COS NPs were added and resuspended in the buffer solution through vortexing (and mild sonication if necessary). The NP mixture was stirred overnight, before being centrifuged to separate NP from free RGD. BCA assay was performed on samples of supernatant to determine binding efficiency of RGD to the NPs. NHS concentration across all samples and standards were kept constant for BCA assay analysis, due to the affect and interference of NHS (by reducing the Cu compound in BCA reagent).

2.6 PLGA-CUR NPs

2.6.1 Synthesis

CUR-encapsulated PLGA NPs (PLGA-CUR NPs) were prepared by emulsion method, similar to void PLGA NPs (Section 2.4). CUR was dissolved in DCM alongside PLGA (1:10 CUR:PLGA, w/w), then added to the aqueous solution containing PVA. After emulsion and stirring to evaporate DCM solvent, the NP mixture was filtered through Whatman Grade 1 filter paper to remove precipitated and aggregated CUR, before centrifugation and washing steps.

2.6.2 Encapsulation Efficiency

Due to the hydrophobic nature of CUR, indirect measurement of encapsulation efficiency (EE) and drug-loading efficiency (DL) through the supernatant post-synthesis was not feasible. Instead, a known mass of lyophilized CUR-loaded NPs were dissolved in organic solvent. These samples were analysed via UV-Vis absorbance plate reader and compared against a standard curve of CUR (100 – 10,000 ng/mL) dissolved in ACN. The calculated concentration was compared to the initial amount of CUR and theoretical maximum encapsulation concentration (10% NP mass, based on the synthesis parameters) to determine EE% and DL%, respectively.

$$\text{EE\%} = \frac{\text{Measured encapsulated CUR conc.}}{\text{Maximum encapsulated CUR conc.}} * 100\%$$

$$DL\% = \frac{\text{Measured encapsulated CUR mass}}{\text{Total NP mass}} * 100\%$$

2.6.3 Degradation and Release Study

CUR-encapsulated NPs were resuspended in 50 mL PBS buffer (pH 7.2) to 2500 ng/mL (or 500 ng/mL) CUR, using DL% of the NPs to find the required mass of NPs to achieve desired concentration. This solution was stirred, and 1 mL aliquots were taken at various time points for up to 72h. These aliquots were treated based on the experiment: either CUR within only the supernatant, only the NP pellet, or the entire solution was measured. Degradation of CUR in NPs vs free CUR measured the drug within the entire solution; this simply required dilution with ACN followed by centrifugation (20,000g for 5 min) to remove any insoluble precipitate. Samples were then transferred to UPLC vials for analysis. Supernatant or NP pellet samples were prepared by separating the two via centrifugation (20,000g for 5 min), to separate free CUR from NP pellet. The supernatant was then mixed with ACN to match UPLC mobile phase composition and transferred to UPLC vials. If NP pellet content was to be measured, ACN was added to fully dissolve

PLGA NPs, then diluted with buffer to mobile phase composition and transferred to UPLC vials. CUR was quantitated against a standard calibration curve from 50-4000 ng/mL.

2.7 Cell Uptake Study

The cell uptake study was designed to assess the effectiveness of the COS-RGD-coated NPs at targeting tumour cells versus bare PLGA NPs. RGD peptides have previously been shown to effectively target OVCAR-3 human ovarian carcinoma cells; thus the cell line was used in this study.[110] To better visually compare treatments, Coumarin-6, a hydrophobic fluorescent dye, was used as a replacement encapsulant to CUR. Coumarin-6 achieves peak excitation around 457 nm.

Briefly, OVCAR-3 cells were cultured and then seeded in a 96-well plate, letting cells incubate for 24 h at 37 °C and 5% CO_2. Coumarin-6 in PLGA NPs, PLGA-COS NPs, PLGA-COS-RGD NPs, or free Coumarin-6 (1000 ng/mL) was suspended in cell medium and added to the wells, incubating for another 24 h under the same conditions. The plates were washed with PBS solution, then cells were fixated with formaldehyde solution (4%), and finally stained with DAPI solution (300 nM) for 5 mins. The plates were once again washed with PBS and then imaged with fluorescent microscopy. The DAPI stain and Coumarin-6 each showed up under separate channels. ImageJ was used to quantify average fluorescent intensity of Coumarin-6 within cells to determine relative uptake (N=5 cells were sampled in each treatment well).

2.8 Cell Toxicity Study

As a further demonstration of the delivery effectiveness of PLGA NPs, OVCAR-3 cells were treated with NP-encapsulated and free CUR for up to 24 h. The different treatments were compared with varying CUR concentrations (between 2.5-40 µg/mL) and treatment times (between 2-24 h). To isolate the effects of the delivered CUR and the NPs themselves, OVCAR-3 cells were also treated for 24 h with void NPs, at the highest and lowest void NP concentrations equivalent to the loaded NP treatments. This void

treatment would help determine if the NPs were contributing to cell toxicity directly, in addition to their delivery of CUR drug. Each treatment group was performed in triplicate (N=3).

OVCAR-3 cells were seeded in a 96-well plate at 5000 cells/well and incubated for 24 h at 37 °C and 5% CO_2. Treatment medium was produced by resuspending NPs in cell culture medium; free CUR treatment medium to assist in dispersion of CUR, which was insoluble in the aqueous medium. After incubation of cells, old medium was replaced with treatment medium, and the cells were incubated under the same conditions as prior (for 24 h in all non-time-dependent studies). After treatment incubation, cells were washed several times with PBS to remove residual CUR; MTS assay was then performed with Promega CellTiter 96™ AQueous One Solution Cell Proliferation Assay, following the recommended protocol. Colourimetric results from the MTS assay were quantified with Varioskan microplate reader.

2.9 Statistical Analysis

Experiments were conducted in at least triplicate. Data was statistically analysed by unpaired t-test and one-way ANOVA where applicable. The value of $\alpha = 0.05$ was used to determine whether results were statistically significant.

3 Results and Discussion

3.1 Chitosan Oligomer Characteristics

To maximize yield per batch, the maximum amount of chitosan per unit volume that would retain consistent, productive results was explored. Based on studies, it appeared that the main factor determining degree of depolymerization for nitrous acid depolymerization was the ratio of nitrous acid to GlcN units.[50,52] Neglecting slight variations in weight due to differences between end groups and monomer units within the polymer chain, estimating the molar quantity of GlcN units could be simplified by assuming and dividing the weight of the chitosan by the MW of GlcN; estimating the molarity of the chitosan itself was unnecessary. Thus, this aspect was not a factor in determining whether to use high or low MW chitosan as a starting reagent. Low MW chitosan was ultimately chosen due to its favourable solubility; low MW chitosan also likely resulted in lower viscosity than high MW chitosan per unit mass dissolved.

Another aspect of consideration was the increase in viscosity as more chitosan was added. Viscosity limited the ability of the stir bar to effectively mix the experimental solution, especially after addition of nitrous acid for even dispersion. Most importantly, however, before limitations with mixability became an issue, the viscosity posed an issue for degassing of the solution. The nitrite in nitrous acid reacts with dissolved oxygen to form nitrate, changing the stoichiometric ratio of NO_2 to GlcN units, and affecting the average oligomer length.[111,112] Degassing of the mixture is necessary to minimize this side reaction. The most straightforward method available was vacuum degassing in a vacuum chamber. At lower viscosity, bubbles of dissolved gas would form in the liquid and rise before being removed by vacuum. As viscosity increased, these bubbles would move noticeably slower. At higher viscosities, these bubbles would remain even after several hours under vacuum. It should be noted that most nucleation sites for these bubbles seemed to occur at surfaces; thus, this issue was lessened by removal of the stir bar during degassing, lowering total surface area near the bottom of the chitosan solution. Chitosan could not be introduced after degassing, as the mixing action would simply reintroduce dissolved gas back into the solution. Further acidification of the mixture did lower viscosity, but this potentially introduces variance in the COS product

as hydrochloric acid has been used in both the de-acetylation and depolymerization of chitosan.[113,114] It was determined that 200 mg/mL low MW chitosan was the maximum acceptable concentration.

Depolymerization was successfully confirmed with ^{1}H NMR spectroscopy. The presence of the amf end unit is confirmed by the small peak at 5.01 ppm that corresponds to the aldehyde proton, as well as peaks at 4.05, 4.15 and 4.36 ppm. ^{1}H spectra are corroborated by NMR data of COS from the Moussa study[50,52]. By comparing the integrated areas under H-2 GlcN to H-1, 3, 4 or 5 amf proton signals in Figure 3-1, we can see that the average length of each COS molecule is around 20 GlcN units to every amf end unit. Control of the average length of COS was shown to be relatively replicable; average of triplicate samples of COS using a 10:1 GlcN/$NaNO_2$ molar ratio showed an average observed length of 21.8 ± 1.8 units. Stoichiometric control was further confirmed by increasing the amount of $NaNO_2$ and observing a change in average oligomer length; average of triplicate samples of COS using a 10:1 GlcN/$NaNO_2$ molar ratio showed an average observed length of 10.6 ± 2.4 units.

The successful attachment of adipic hydrazide to COS through the amf aldehyde group is confirmed by the absence of the aldehyde peak (5.01 ppm) as the reaction site, as well as the presence of peaks at 1.57 and 2.31 ppm that correspond to the aliphatic carbon chains between the hydrazide groups, as seen in Figure 3-2.

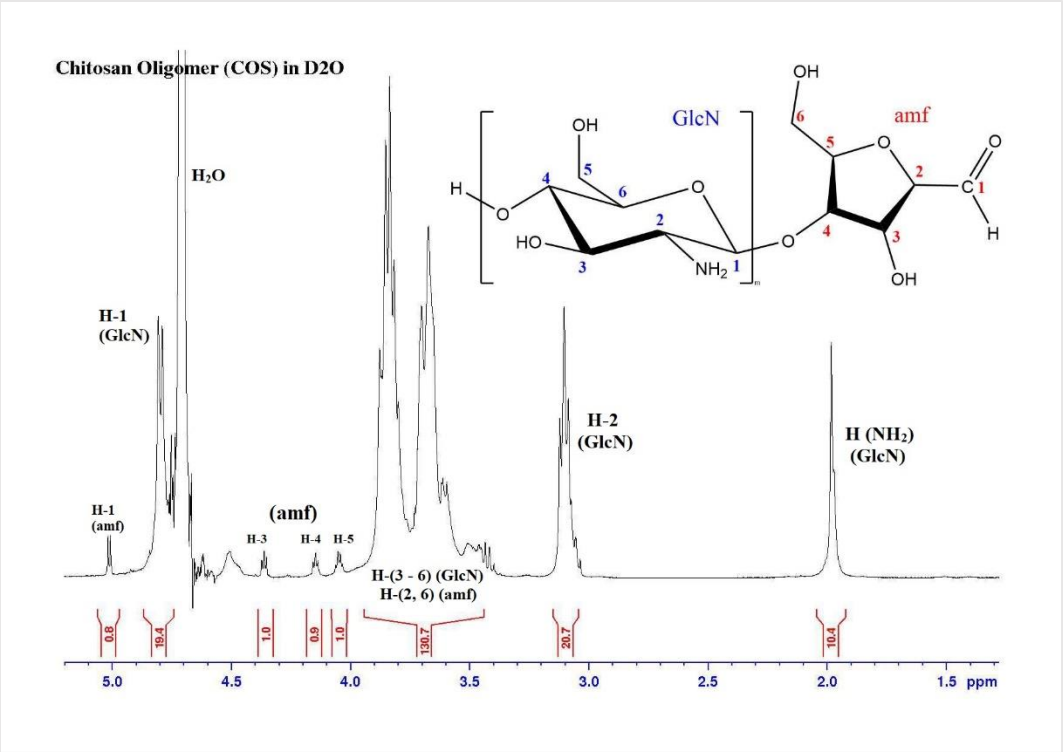

Figure 3-1: ^{1}H NMR spectrum of COS sample, with GlcN to amf ratio of 20. Spectrum processed and created in TopSpin.

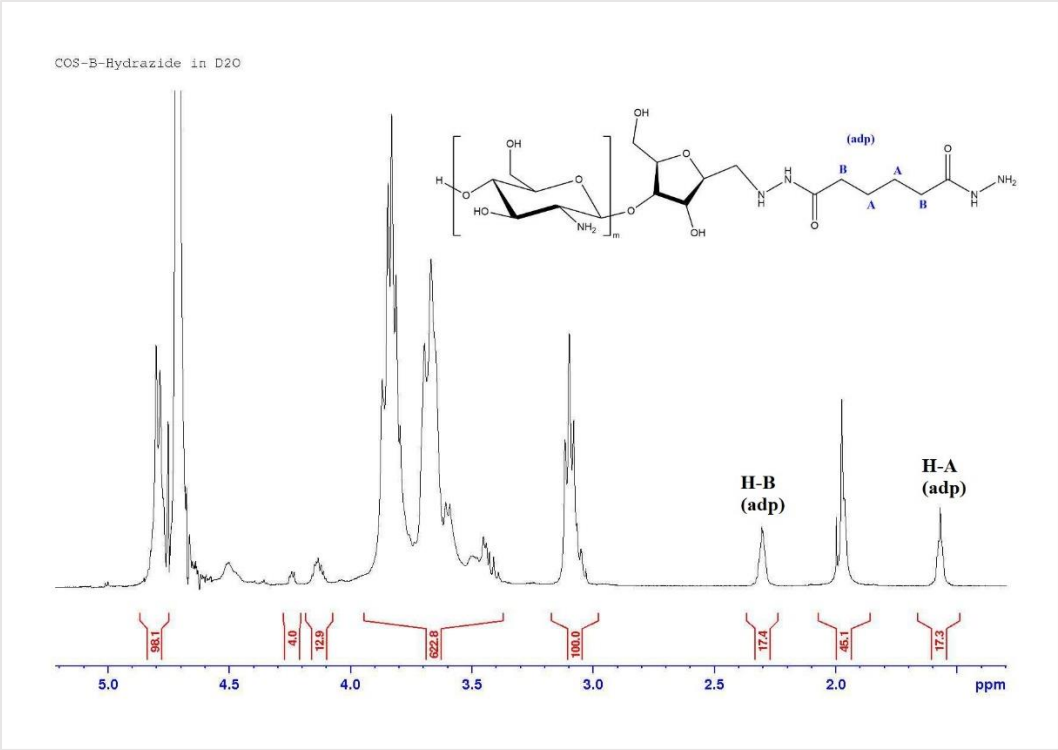

Figure 3-2: ^{1}H NMR spectrum of COS-hydrazide sample. Spectrum processed and created in TopSpin.

MALDI-TOF MS of COS samples did show observable differences between COS produced by depolymerization with different stoichiometric molar ratios of GlcN to $NaNO_2$. In line with NMR results, chitosan depolymerized with more $NaNO_2$ results in a higher degree of depolymerization; in Figure 3-3 there is much less signal after around 1000 m/z in the COS sample with a 4:1 GlcN to $NaNO_2$ ratio, with almost no observable signal discernable from noise past 1500 m/z. This is compared to the COS sample with a 10:1 GlcN to $NaNO_2$ ratio, which still contains significant signal around 1500 m/z, with signal-to-noise ratio still quantifiable up to almost 2000 m/z.

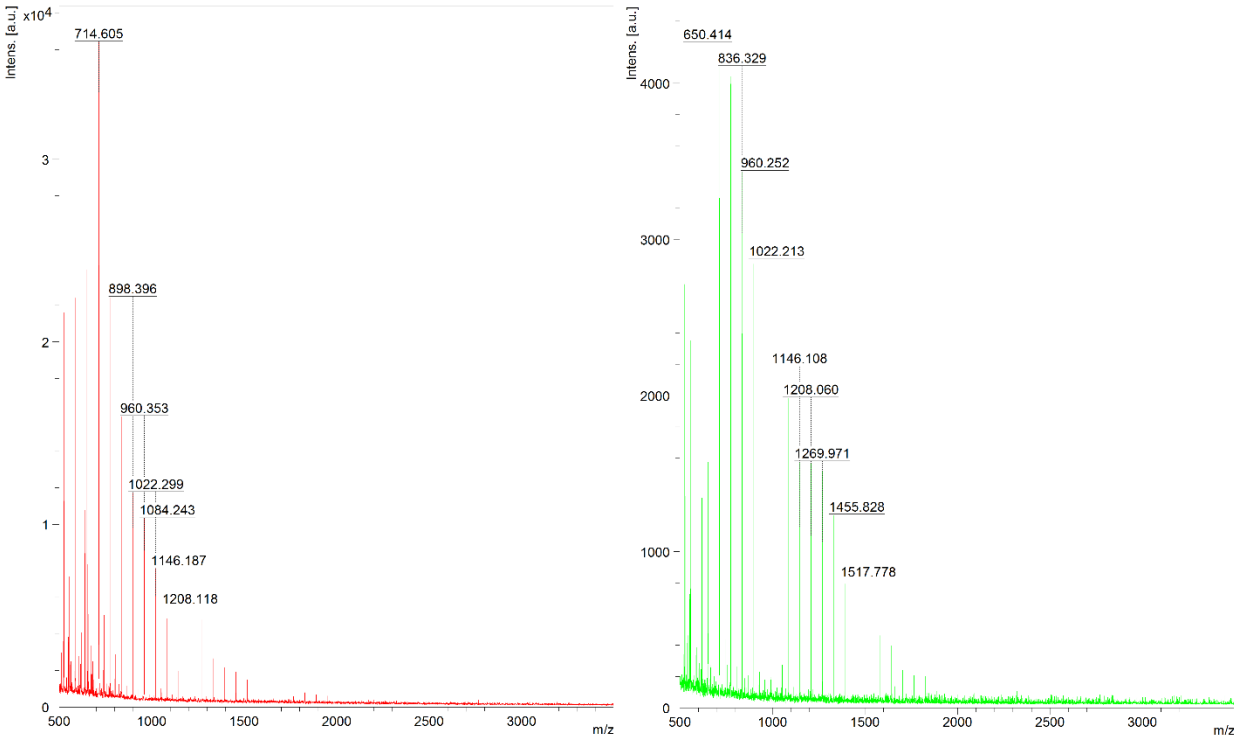

Figure 3-3: MALDI-TOF MS of COS samples synthesized with different GlcN to $NaNO_2$ ratios (Left – 4:1, Right – 10:1).

However, beyond the general trend of relative size, it is difficult to analyse this MS data for specific information such as size distribution, weight-averaged oligomer length, etc. There are generalizations that can be made, but a significant issue comes from the degree of acetylation of chitosan. Acetylated and de-acetylated GlcN units vary by the addition of an acetyl group attached to the primary amine. Where a de-acetylated GlcN unit has a MW of 179 g/mol, an acetylated GlcN unit has a MW of 221 g/mol, almost 25% heavier. Even with a degree of de-acetylation close to 85%, this still causes a shift in mass (and therefore signal at a given m/z ratio), which is only exacerbated as the chitosan oligomers get longer and longer.

3.2 NP Characteristics

PLGA NPs were successfully synthesized by emulsion method; their characteristics were replicated by maintaining consistent parameters including polymer concentration, organic to aqueous ratio, PVA content, and sonication intensity. Similarly, PLGA-COS NPs were also prepared, and both were characterized by size, PDI and ZP (zeta potential) via Zetasizer. During preparation of the PLGA NPs, it was important to find an optimal PLGA concentration in the DCM organic solvent solution. The lower the PLGA concentration, the lower the overall yield; if the concentration of PLGA was too high, however, this would affect the workability of the solution. The two main issues observed were that, when PLGA concentration was increased, the viscosity of the solution would also increase – past a certain viscosity, this made workability (i.e. transport/aliquoting via pipette or syringe) more difficult. A decrease in consistency was also observed for high PLGA concentration samples; in some samples, emulsions would break at some point during the hardening process, while in other samples, PLGA would precipitate to bulk as soon as the organic solution was added into the aqueous medium. It was found that 50 mg/mL PLGA in DCM was the highest viable concentration to maintain yield and consistency.

Another factor in the successful synthesis of PLGA NPs was the sonication parameters, mainly the amplitude. Total sonication time was 90 s to ensure full emulsion was achieved across the entire mixture; higher sonication time would likely be required for larger volumes and vice versa. It should also be noted that prolonged sonication could adversely affect the NP product, as such exposure to high levels of energy and agitation could induce degradation in the polymer, to the coating, or even to the encapsulated drug. Pulse times were set to 15 s on, 5 s off; this prevented excessive amounts of heat from the sonication process from causing variance in the emulsion process. Sonication amplitude is important because a certain amount of energy and agitation is required to break up the PLGA/DCM mixture in the aqueous medium into nanoscale droplets. A trend was reported that showed decreasing NP size with increasing sonication amplitude; however, this trend eventually reaches a plateau.[115] Initially, amplitude was set to 80% for this study. Though this would provide a desired NP size in some cases, these sample emulsions were sometimes

prone to premature aggregation/coalescence. When amplitude was reduced to 60%, NP size range remained acceptable, without the tendency for premature aggregation. One possibility is that higher sonication amplitude provides more energy, meaning faster NP movement and more frequent collisions. At high enough energies, these collisions may result in nanodroplets overcoming repulsive forces, and aggregating together once more. At a certain point, the benefit of this high energy agitation breaking up large droplets is outweighed by the increased frequency of successful aggregation collisions.

Both PLGA and PLGA-COS NPs have a similar size (less than 300 nm average), and a relatively narrow PDI (around 0.1). The COS coating did not appear to affect the size of the NPs significantly, though there seemed to be higher variance and a slightly wider PDI. The negative ZP of PLGA NPs is likely mainly due to the carboxyl end groups of PLGA molecules at the surface of the NPs. The positive ZP of PLGA-COS NPs suggest the successful coating of COS to the PLGA NP surface, due to the presence of positively charged amine groups in COS.

*Table 3-1: Zetasizer results of PLGA, PLGA-COS NPs. *NP results containing encapsulated CUR. Fluorescence of CUR negatively affects results.*

	Z-avg size (d, nm)	PDI	Zeta Potential (mV)
PLGA NPs	221.7 ± 19.7	0.085 ± 0.054	-15.2 ± 0.7
PLGA COS NPs	229.2 ± 50.2	0.119 ± 0.056	+26.1 ± 1.2
PLGA NPs (w/ CUR)*	281.2 ± 23.4	0.238 ± 0.060	N/A
PLGA COS NPs (w/ CUR)*	278.8 ± 102.0	0.195 ± 0.080	N/A

When comparing PLGA NPs with and without encapsulated CUR (via t-test), there was a statistically significant difference NP size and PDI. Comparisons between samples of PLGA COS NPs with and without encapsulated CUR did not conclude a statistically significant difference. These results, however, should be

taken with a grain of salt; CUR exhibits some fluorescent properties, which caused interference with both the DLS and ELS techniques employed by the Zetasizer. The fluorescence filter in the Zetasizer did seem to help with DLS size analysis to a degree, but efficacy was inconsistent. ZP attempts with the CUR-encapsulated NPs were highly inconsistent. It is unclear how much of this contribution was due to CUR fluorescent interference, or if the CUR itself was playing a role on the NP surface.

One issue of particular notice in early sample groups was aggregation of NPs after centrifugation. The NPs were able to remain stable and suspended in aqueous solution over relatively prolonged periods (aggregation was not observed over 72 h in some samples left over weekends), but the increased forces (15,000x g) accelerated aggregation by overcoming repelling forces of the NPs. Some NPs were still recoverable by agitation through vortexing. This was confirmed by taking DLS measurements of void PLGA NPs before centrifugation, then taking measurements of the same void NP samples after centrifugation. These post-centrifugation samples were vortexed for 30 s, then centrifuged at very low speed (<200 g for 1 min), such that aggregated PLGA would quickly sink to the bottom, while remaining NPs would remain suspended in solution. Comparison of these measurements saw no discernable difference in NP size across tests. While this was encouraging for viable measurement data, this obviously meant a sizeable reduction in yield (from around 70% post-lyophilized yield, to less than 20% if the aggregated NPs were removed).

This centrifugation step is necessary in the purification and washing of NPs from reagents. There were ways to subvert this issue, with one possible alternative being to switch from centrifugation to dialysis to wash and purify the NPs. While this change would have solved the issue, it would constrain throughput of synthesis of NPs. Space would be a significant issue, as each sample group would require a vessel and stir plate of adequate size, which would be occupied for the duration of the dialysis step. This dialysis step would need to be performed every time the NPs needed to be washed, purified, or changed mediums. Despite this method taking up a large amount of space and far more time than centrifugation, it would not address the underlying issue: that the PLGA NPs were potentially still relatively unstable, which might

have resulted in increased aggregation during long-term storage or the coating processes of COS and/or RGD.

Instead, a solution was found in a change to the formulation of the NPs, particularly in the surfactant. As the surfactant, PVA is able to stabilize the formation of NPs through its interactions with both the aqueous and organic domains. The presence of the surfactant introduces an energy "barrier" that must be overcome with respect to the Gibbs free energy at the interface between the two mediums.[116] Without this barrier, an emulsion mixture would be unstable, spontaneously coalescing back into macro droplets over time. This stabilising effect increases with increasing surfactant concentration, up to the critical micelle concentration (cmc). Increasing the PVA concentration was considered; however, studies showed conflicting reports of increasing PVA concentration both increasing and decreasing particle size.[117–119] Another aspect of emulsion stability lies in the intermolecular forces at play. Stability requires the NP surfaces to resist van der Waals attraction through either electrostatic or steric repulsion. Steric repulsion is the force that allows non-ionic polymers like PVA to maintain stable emulsion mixtures.

One study that showed that the type of PVA used as a surfactant could affect NP stability. This study explored both degree of polymerization and degree of hydrolyzation, and found that the degree of hydrolyzation was most important in providing the best NP stability.[120] The basis of this mechanism was that PVA on the surface of NPs would interact with each other, and that hydroxyl groups of hydrolyzed portions of the PVA chain would exhibit strong hydrogen bonding with each other, encouraging aggregation and the formation of a gelled network. Inversely, the non-hydrolyzed acetoxy groups would in a steric repulsive manner. The study showed that PVA gelatinization required a higher concentration of organic solvent (acetone) in grades of less hydrolyzed PVA. Thus, PVA was switched from 98-99% hydrolyzed grade to 87-90% hydrolyzed grade, which improved redispersion and stability post-centrifugation.

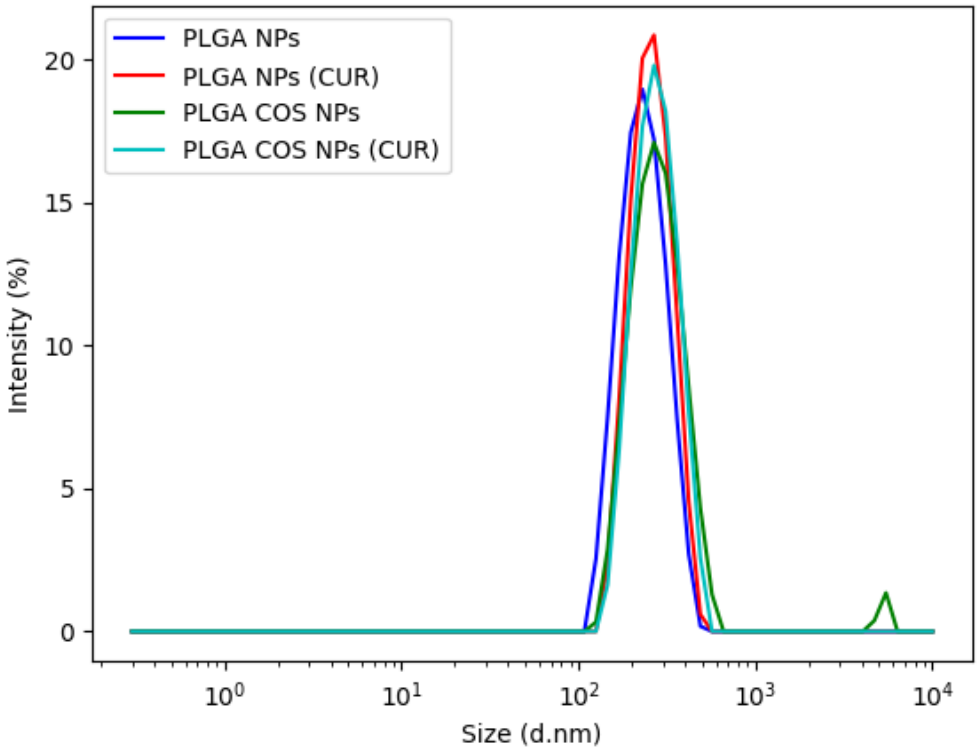

Figure 3-4: A sample of Zetasizer DLS results showing size distribution of PLGA and PLGA-COS NPs, with and without CUR encapsulation.

A representative size distribution from each NP sample group is shown in Figure 3-4. While mostly consistent, some samples did show some smaller peaks at higher size ranges, such as the one shown at around 6000 nm. This was more of an issue with PLGA COS NPs than PLGA NPs. This seems to suggest the introduction of some level of instability with the addition of COS. It is plausible that this level of instability is a result of similar mechanisms to the PVA issue described prior. The hydroxyl and primary amine groups present along the polymer chain likely contribute to instability through hydrogen bonding; the acetylation of the amine groups may contribute to increased stability through improving steric repulsion. It would follow that higher percentage N-acetylated chitosan would result in better overall NP stability. However, optimization of this process would need to consider the following: deacetylated amine groups

are necessary for the next step – covalent binding of the RGD peptide to the COS-coated NP surface. Additionally, hydrogen bonding is an important factor in aqueous solubility; N-acetylation also reduces the already poorly soluble state of chitosan.[121,122]

COS-coated PLGA NPs were analysed through ^{1}H NMR spectroscopy. However, peaks characteristic of COS (see Figure 3-1) were absent. As shown in Figure 3-5, the major distinct peaks for COS from 3.5 – 4.0 ppm do not show up in the ^{1}H NMR spectrum of PLGA-COS NP samples.

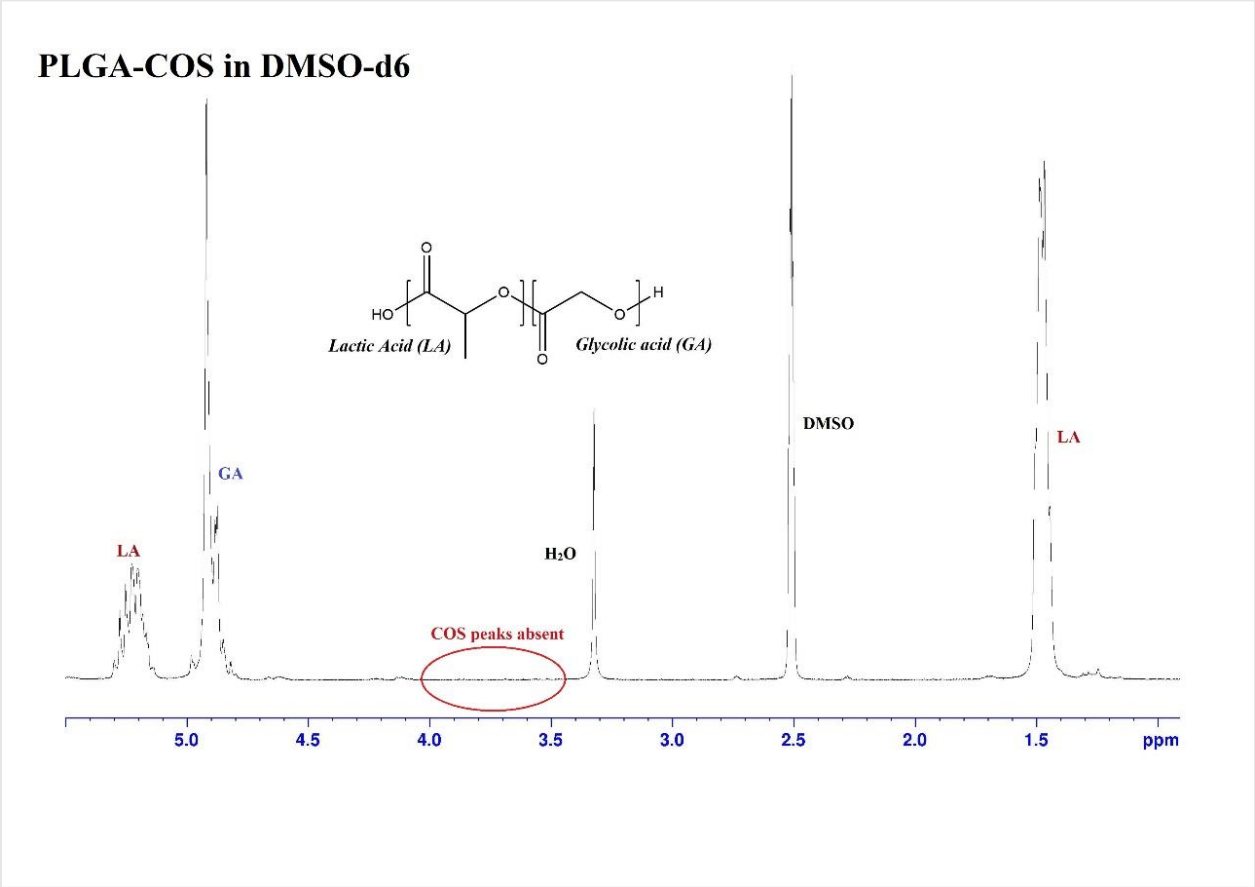

Figure 3-5: ^{1}H NMR spectrum of PLGA-COS NPs in DMSO-d6. Spectrum processed and created in TopSpin.

Since the positive ZP on the surface of the NPs as analysed via Zetasizer indicates the presence of COS, it is possible that there are other factors that explain this absence. The first possibility is that the

amount of COS is so small compared to PLGA, that the relevant peaks are too low to be resolved at the required concentration. The second possibility is that the PLGA-COS that is formed by chemical conjugation is relatively insoluble in organic solvents required to dissolve PLGA alone (this factor may work in tandem with the former). The third possibility is that COS is not chemically binding to the surface of the PLGA NPs, and instead remains physically adsorbed – thus, once the NP structure is destroyed by dissolution in organic solvent, the now free COS is completely insoluble in the organic solvent and thus undetectable by NMR.

RGD coating onto PLGA-COS NPs were confirmed by BCA assay of both the supernatant solution, and the NPs directly. Due to the interaction of NHS with the BCA reagent causing the same Cu reduction and colour change, three different standard curves were analysed (shown in Figure 3-6**)** to ensure accuracy of results. The standard curve results confirm that NHS interference with BCA assay is consistent and predictable, and that maintaining the same concentration across samples/standards minimizes potential variance due to its presence. The supernatant samples, which contained NHS from the binding reaction, were analysed against the RGD standards containing 12 μg/mL NHS, and diluted appropriately to match this concentration. The NP samples, which were centrifuged and washed of residual reaction reagents, were analysed against RGD standards without NHS. The assays showed a 12.9% ± 0.4% binding efficiency.

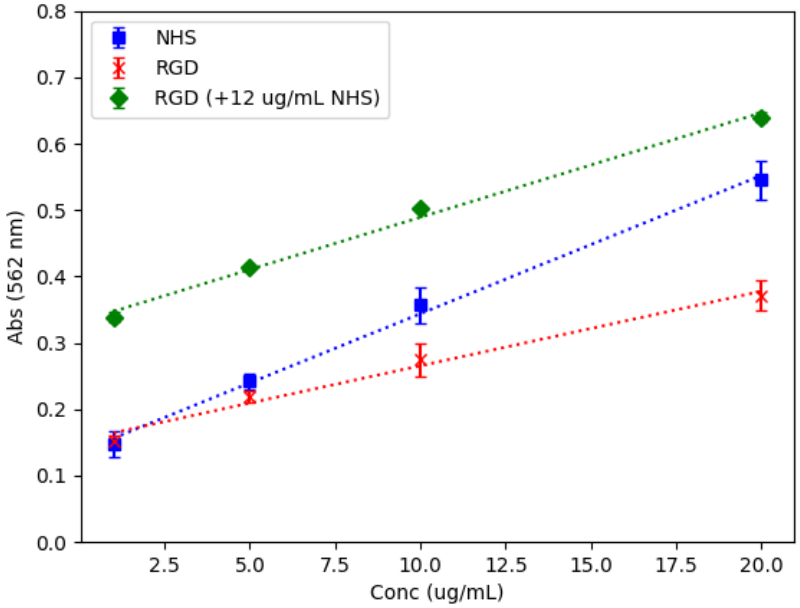

Figure 3-6: BCA assay standard curves – NHS, RGD, and RGD with controlled NHS conc.. All standards prepared in 100 mM MES buffer, pH 5, N=3. R^2 > 0.99 for all standard curves.

3.3 Curcumin-Loading Results

3.3.1 Drug Loading and Encapsulation Efficiency

Samples of CUR-loaded PLGA NPs were dissolved in 3 different organic solvents (ACN, ethyl acetate, chloroform) to ensure full extraction of CUR from NPs. Each sample was dissolved to an initial concentration of 1 mg/mL (NP mass) and performed in triplicate. At 100% theoretical EE, the NPs would contain 10 µg/mL CUR. The results are shown in Table 3-2. Regardless of solvent as dissolution medium, the results indicate just under 6 µg/mL CUR, which equates to 6% drug loading (DL) or 60% encapsulation efficiency (EE).

Multiple organic solvents were used to confirm EE; since the cryoprotectant trehalose was incompatible with most organic solvents, samples of encapsulated NPs were freeze dried without the sugar. This resulted in significant aggregation of the PLGA which remained partially insoluble in various organic

solvents even after prolonged sonication. This undissolved polymer was visible as solid white particulate. It is suspected that this was due to the presence of PVA remaining in the NPs, which may have formed a network and shielded some of the NP material inside the aggregate from being dissolved in the organic solvent. The amount of aggregation as a result of unprotected freeze drying was significantly reduced when PVA was switched from 98% hydrolyzed to 87% hydrolyzed grade. In the newer samples with less hydrolyzed PVA, there was no observed particulate – however, to ensure accurate results and full solubility, EE% testing was still performed with all three organic solvents.

Table 3-2: CUR Drug loading of PLGA NPs through direct dissolution of NP.

Sample (Solvent)	**Avg Conc (µg/mL)**	**SD (µg/mL, n=3)**	**DL%**	**EE%**
Acetonitrile	5.58	0.13	5.58%	56%
Ethyl Acetate	5.95	0.04	5.95%	59%
Chloroform	5.93	0.15	5.93%	59%

These encapsulation efficiency results were below expected values based on similar studies, but within acceptable range for subsequent testing.[65,123] One contributing factor to the lower EE was quality and solubility of the supplied CUR. When dissolved in organic solvent (DCM, ACN or ethyl acetate), a small but visible amount of the CUR remained insoluble, even after prolonged sonication. The CUR supplied was >94% curcuminoid content, but >80% curcumin. It is possible that the insoluble content was insoluble curcuminoid compounds, impurities, or a combination of both. While the drug encapsulated in the NPs was possibly only 80% curcumin by weight, the same CUR was used to create the reference standard curves; thus, it is likely that this deviation carried over and was taken into account by the standard curve. One other possibility is some amount of release/degradation during the NP synthesis, including washing and resuspension steps. CUR was shown to have some minor degradation after 24 h, even with NP encapsulation (further discussed later).

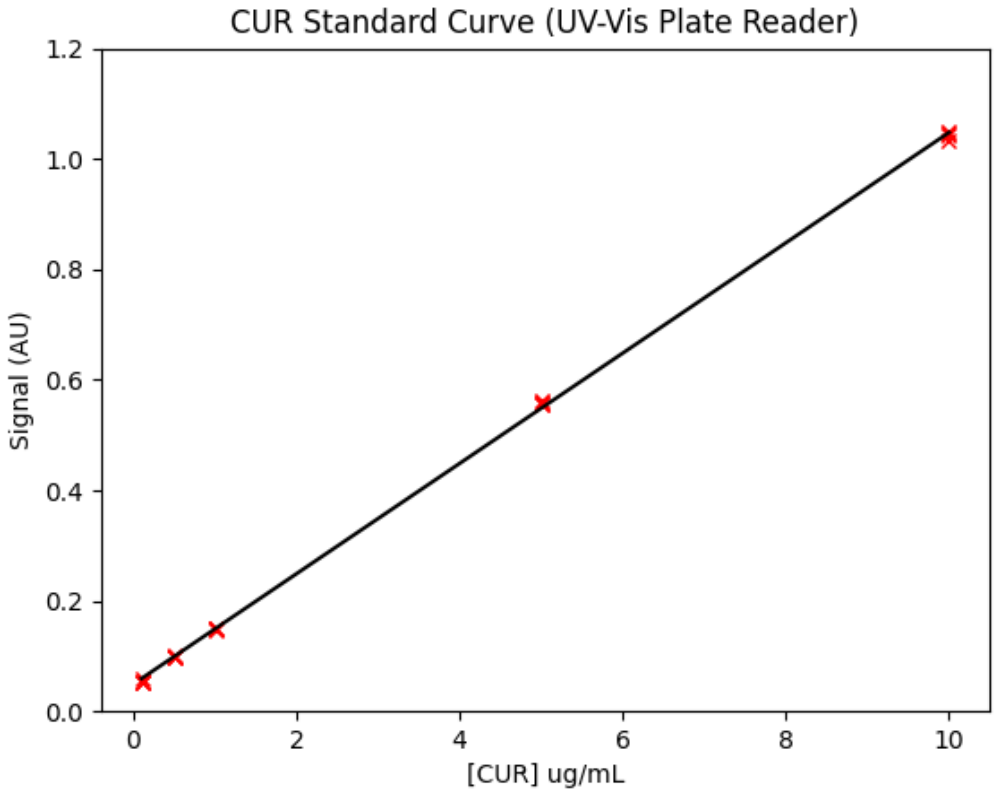

Figure 3-7: CUR standard curve in ACN, from 0.1 – 10 µg/mL. $R^2 > 0.99$

3.3.2 CUR Degradation and Release Studies

Triplicate samples of free CUR, PLGA NP encapsulated CUR, and PLGA-COS NP encapsulated CUR were prepared by suspending lyophilized loaded NPs in PBS 1X (pH 7.2) to a CUR concentration of 2500 ng/mL (free CUR samples were prepared by first dissolving CUR in ACN, then adding to PBS and placing under vacuum to assist in evaporation of organic solvent). These samples were allowed to spin at RT for 70h; aliquots were taken at various time points and analysed via UPLC. These aliquots were mixed with organic solvent (ACN) to break the NPs to release and dissolve the CUR. After 70h, it is clear encapsulated CUR is resistant to aqueous degradation compared to the free CUR control group, as seen in Figure 3-8.

By 70 h, PLGA and PLGA-COS NP-encapsulated CUR degraded to 77% and 66% of its original concentration, respectively; meanwhile, free CUR degraded to the point where it was far below the lowest concentration standard, nearing <1% of its original concentration. PLGA-COS NP did slightly underperform relative to PLGA NP samples, though this could be due to the relatively prolonged processing to add COS-coating affecting encapsulation characteristics.

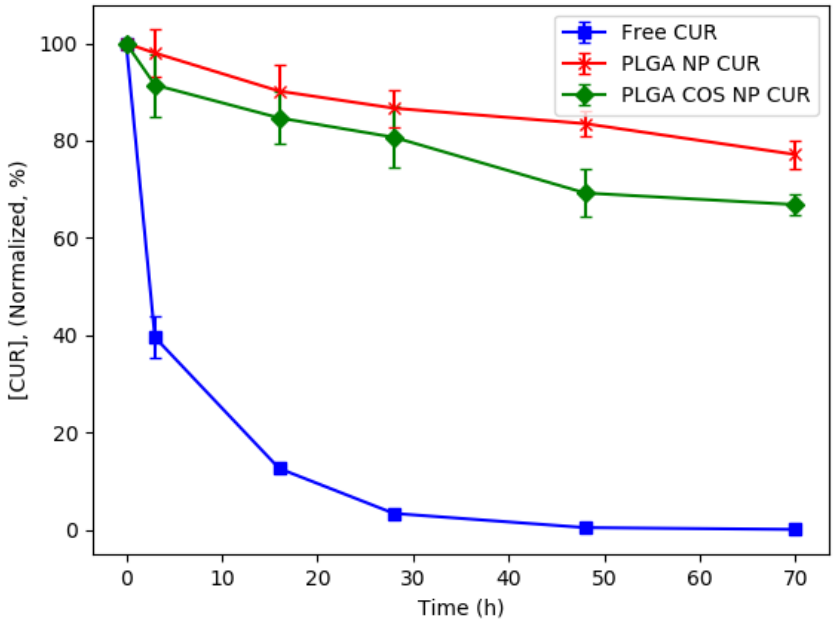

Figure 3-8: UPLC results of degradation of encapsulated CUR compared to free CUR in PBS solution (pH 7.2, at RT).

A similar experiment was conducted to attempt to determine the rate of release of CUR from PLGA NPs; again, samples were prepared as above, except aliquots were centrifuged to separate the NP from the supernatant. While CUR concentration in NP samples decreased gradually, concentration in the supernatant remained extremely low. These results are shown in Figure 3-9. Along with the previous results of free CUR, it seems to suggest that CUR released from the NPs is quickly degraded, even in the buffered solution. There were attempts to quantify the degradation by monitoring metabolite levels; however, it became clear

that this was not feasible for 2 major reasons. The first reason was that CUR has many metabolites and degradation products; it also has several similar derivatives (a family of molecules known as curcuminoids).[124–126] The second reason was that, based on spectral UV-Vis analysis of samples through UPLC, it was difficult to determine definitive peaks of these products, even after relatively significant levels of degradation were shown in CUR concentrations of the samples. It could have been that the degradation products did not have significant absorbance in the viable analysis range of the UPLC system; it could have also been an issue of the by-products degrading further into simpler products (which, again, were unable to show up during analysis). In the future, it may be possible to use UPLC in conjunction with TOF-MS to try to determine the presence and amount of degradation products, perhaps by also utilising a size-based separation column instead.

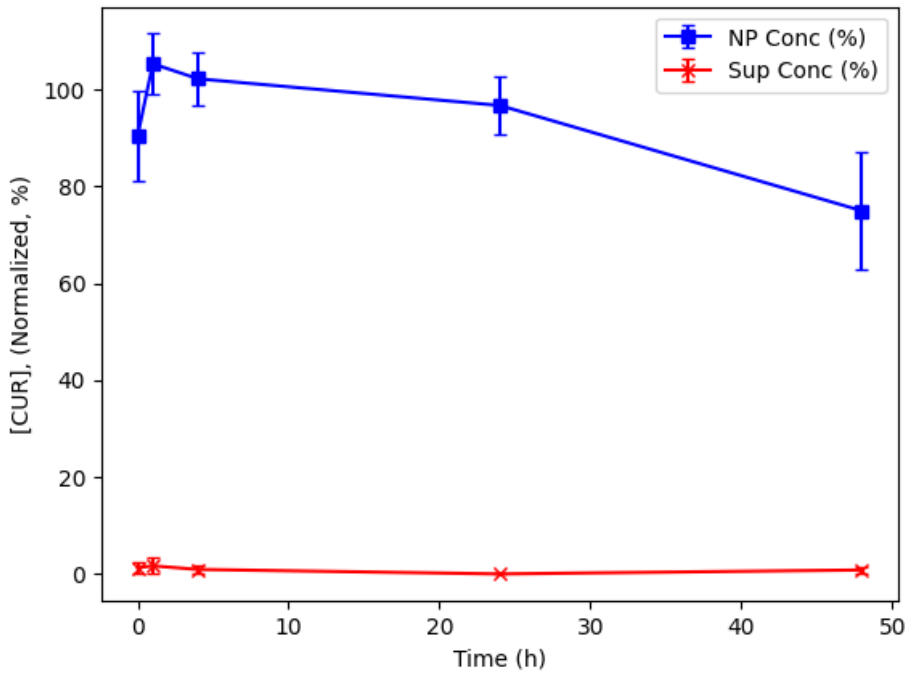

Figure 3-9: Release study comparing CUR amounts in PLGA NPs over time, vs how much is present in the supernatant (Sup). Release study performed in PBS buffer, pH 7.2. CUR signal was absent from supernatant.

Another final experiment regarding CUR release was conducted at a much lower concentration; the 2500 ng/mL concentration initially used was loosely based on sink conditions claimed in other papers.[31,127,128] The main issue was that, several sources claimed that the solubility of CUR was much closer to 600 ng/mL.[129–131] A value of similar magnitude was validated by a quick and simple experiment that involved adding an excess amount of CUR to PBS buffer, letting dissolve for 4 h at RT (assisted by bath sonication to accelerate the process), and then filtering out undissolved CUR and analysing its concentration via UPLC (in PBS buffer, pH 7.2, the maximum solubility of CUR was observed to be approximately 1200 ng/mL). Thus, the experiment involved NP samples with CUR concentration of 500 ng/mL (starting at a lower concentration to emulate more accurate "sink conditions" was not feasible, as it was difficult to accurately quantitate levels of CUR below 50 ng/mL). This experiment, however, ran into similar problems regarding the release of CUR into the PBS buffer supernatant and inability to detect CUR due to degradation.

To more accurately assess the CUR released into solution, the release study was performed in PBS buffer, this time with Tween-80 (T-80) surfactant. Several studies looking at the release of CUR from PLGA NPs utilised 0.5% T-80 (v/v) in their buffer solutions.[65,123,127] The addition of surfactant was likely used to increase solubility of CUR, as well as improve stability in solution. At 0.5% T-80, CUR solubility increased from 1200 ng/mL to over 25,000 ng/mL, around 20-fold increase. CUR also remained detectable in supernatant over the timespans required for the release study (48+ h).

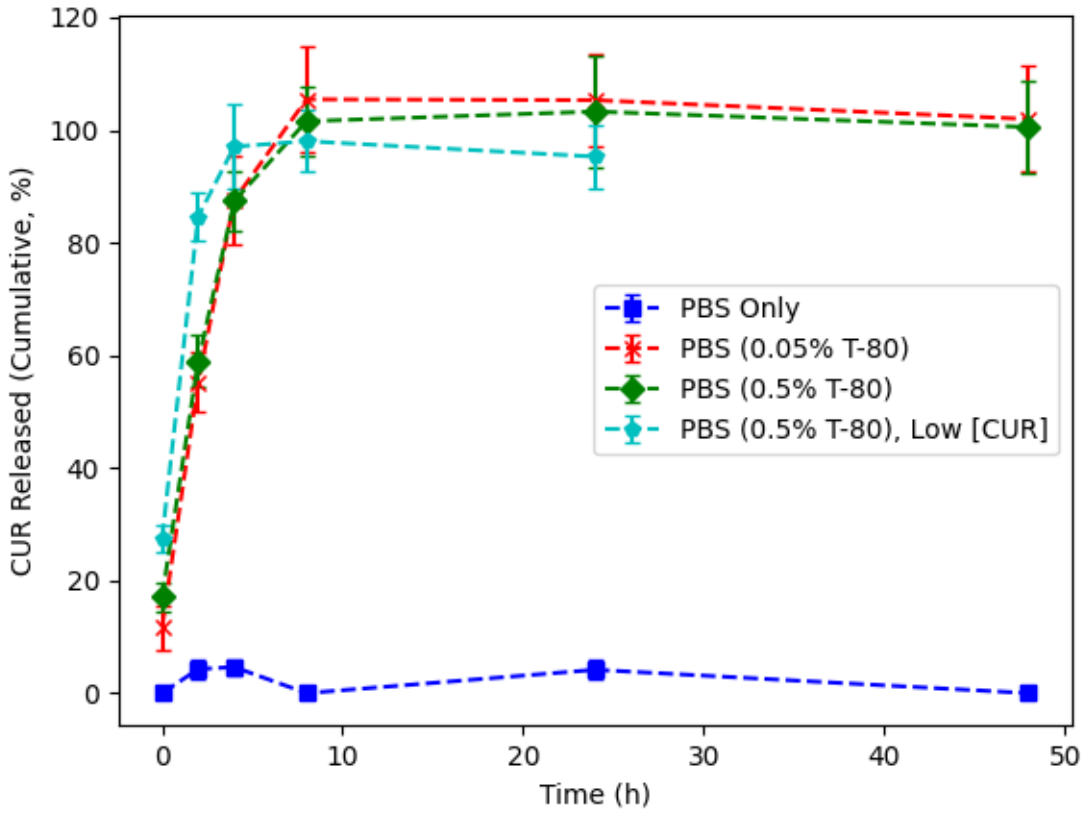

Figure 3-10: Comparing cumulative release of CUR (2500 ng/mL total) from PLGA NPs into supernatant – PBS buffer, with varying levels of Tween-80 surfactant, over 48 h. Low CUR concentration: 500 ng/mL.

In order to determine whether the presence and amount of T-80 affected the release rate of CUR (beyond affects seen from improving solubility), two sample groups of PLGA NPs (at 2500 ng/mL CUR) were prepared in PBS buffer solution with T-80; one contained 0.5% T-80, the other contained only 1/10th the amount of T-80 (0.05%). From Figure 3-10, which shows the concentration of CUR found in aliquots of the sample supernatant, there does not appear to be any difference in release rate between the two concentrations of T-80. Additionally, between 24 and 48 h, there is no significant decrease in the concentration of CUR in the supernatant, indicating that the T-80 also aids in the aqueous stability of CUR. The addition of T-80 was also applied to the release study of CUR in PLGA NPs at the lower concentration

(500 ng/mL CUR). While release was noticeably faster, this sample group followed the same trend of release as the high CUR concentration PLGA NP sample groups. From these release studies at sink conditions, it appears that PLGA NPs completely released their payload of CUR by the 8 h mark. This stands in stark contrast to the results obtained in other studies that appeared to show prolonged and sustained release of CUR over the course of several days.[65,123,127]

From the phrasing of the PLGA NP CUR release studies referenced, it appears that cumulative release of CUR was measured at given time points by centrifuging the whole sample of NPs, measuring the CUR content in the supernatant, and then resuspending the NP precipitate in fresh buffer solution. In contrast, this study used the same solution over the experimental period, and measured CUR content using small aliquots of the solution that were centrifuged to separate supernatant. This was partially done to minimize centrifugation and redispersion of the NP samples, as repeated centrifugations had led to some instability and aggregation, leading to potential inaccuracies in the release profile. This was particularly pronounced before the transition to the lower hydrolyzed grade PVA, but a small amount of visible particulate was present even after the transition. Based on these results, it is likely that the "sustained", steady release observed at the higher concentration samples (as well as the other studies) was instead a steady release of CUR until saturation of the aqueous medium; as free CUR degraded in solution at a relatively steady rate, encapsulated CUR would release to replace it. It seems plausible that the sustained, linear release profile of some of the studies was due to the solution reaching the same saturation point of CUR relatively quickly, but then refreshed in a new buffer solution at constant time intervals (usually 24 h). The constant saturation coupled with the constant time intervals would make it appear to be providing linear release.

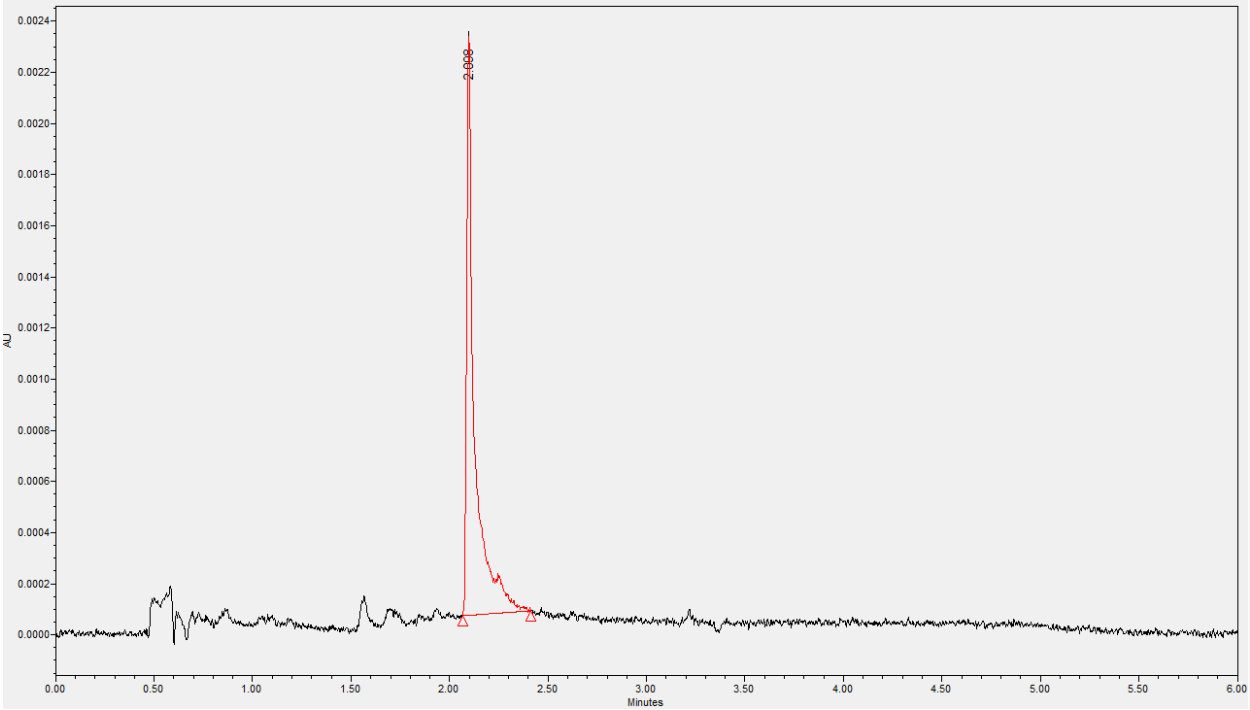

Figure 3-11: Sample UPLC chromatograph of CUR peak (highlighted red). Elution time (x-axis) spans 6 min; y-axis is relative absorbance units (AU). Created in Waters Empower software.

UPLC parameters were optimised to avoid overlap with small impurity signals (as shown in Figure 3-11 from around 0.5 – 1.5 min elution), while still eluting within a reasonably quick time frame (<6 min). Raising the fraction of organic solvent in the mobile phase reduced elution time, but also effectively "compressed" the elution times of all peaks, bringing them closer together. Increasing flowrate also reduced elution time (to a lesser extent than changing organic solvent fraction), but importantly also helped to narrow elution peaks. Balancing flowrate and mobile phase composition was also important in managing the system backpressure – if system backpressure was too high, this would cause premature wear and tear to the UPLC column. Mobile phase composition was also programmed on a gradient, to increase organic solvent fraction after elution of the CUR peak to help flush any remaining residual impurities, undesired peaks from the column. NP material did not appear to cause any interference with the CUR signal.

It should be noted that the CUR peak contains a minor tailing artefact. The ideal UPLC peak is symmetrical, but the CUR peak contains an uneven “tail”. While this ultimately results in only a relative minimal loss of accuracy as the peak is still overall very narrow, this could be improved in future runs. Tailing is typically indicative of three main issues, the first being poor solubility from the sample mixing into the mobile phase. This is often a result of the sample medium being of different composition from the mobile phase, usually if the sample is prepared in pure organic solvent. To mitigate this, CUR samples were diluted with PBS buffer to the same organic/aqueous fraction composition as the initial conditions of the UPLC system. Another factor is potentially void volumes caused by poor/degraded column quality, or loose/poorly fit connections within the UPLC system. This is unlikely, as other samples run on the same system showed minimal tailing, and various tests to check connection integrity did not show characteristic signs of poor connections (e.g. leaks, unexpected pressure differentials, etc.). The last, and most likely candidate was mobile phase composition. Some analytes experience tailing due to secondary interactions with silanol groups within silica-based columns; this can often be minimized by lowering pH of the mobile phase.[132] Increasing the fraction of organic solvent effectively lowers the amount of acid from the aqueous buffer solution. However, increasing the concentration of o-phosphoric acid may cause it to precipitate when mixed with such a high fraction of ACN. While unlikely, there is also the possibility of some degradation of CUR when mixed into the acidic mobile phase, as CUR is more sensitive to degradation under acidic conditions. Some studies suggested the use of methanol over ACN, which allowed the necessary amount of acid in the aqueous buffer solution – however, methanol was also less efficient at fully dissolving the NPs, which could have caused issues for the quality of data, as well as the long-term health of the UPLC system.

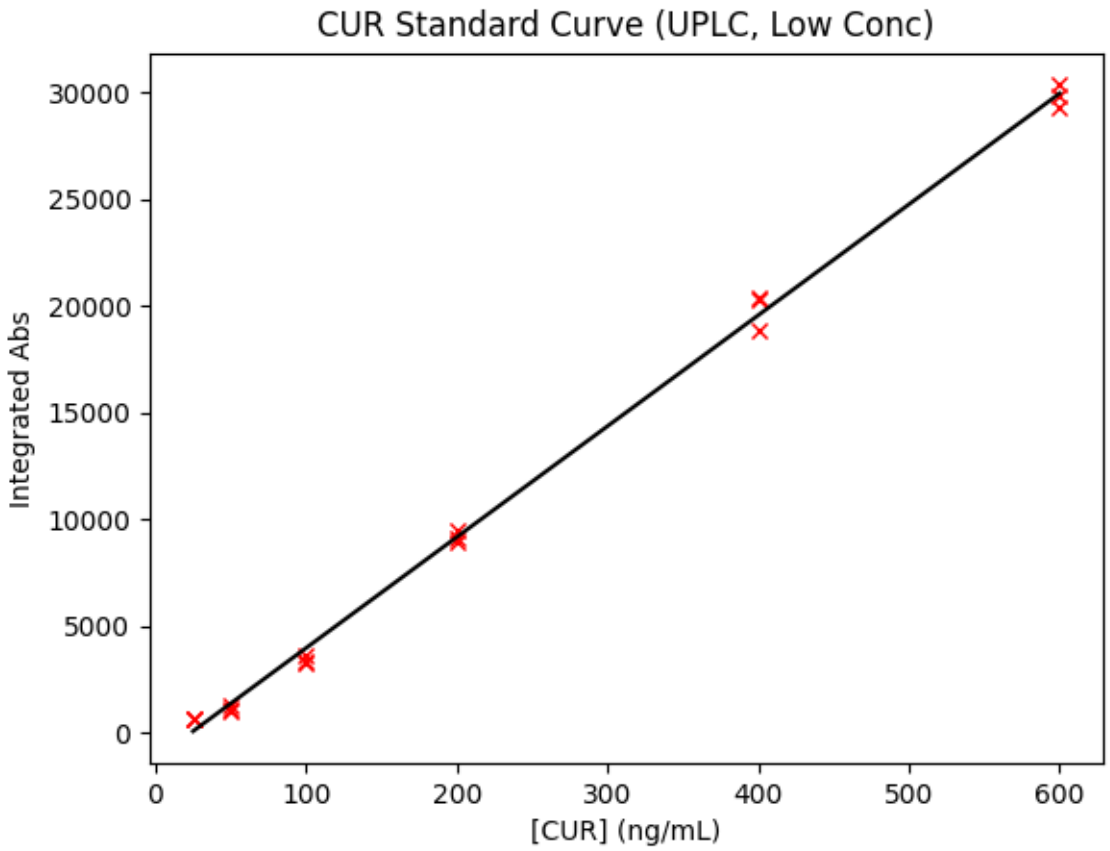

Figure 3-12: Sample of CUR standard curve at lower concentrations via UPLC. $R^2 > 0.99$.

3.4 Cell Uptake Study

Cell uptake of PLGA NP-encapsulated hydrophobic fluorescent dye Coumarin-6 was monitored at various time points up to 24 h. This uptake was compared to a control group with free Coumarin-6. As shown in Figure 3-13, free Coumarin-6 (Group A) was unable to enter the cell even after 24 h of incubation. Meanwhile, Groups B-D (PLGA NP, PLGA-COS NP, PLGA-COS-RGD NP samples respectively) all showed faint fluorescent signal, and therefore successful uptake, even after 0.5 h of incubation.

The fluorescent images of the OVCAR-3 cells were further analysed with ImageJ software; average fluorescent intensity of an image was determined by sampling intensity at 5 different random cells in each

image. Results are displayed in Figure 3-15. Statistical analysis (t-test) determined fluorescent intensity was not significantly different from 8 h to 24 h in Groups B, C or D, suggesting near maximum uptake had been reached by 8 h. Similar analysis between Groups B, C, D showed little statistically significant difference between the overall uptake after 24 h. This seems to suggest that the coated NPs do not provide significant improved delivery over bare PLGA NPs.

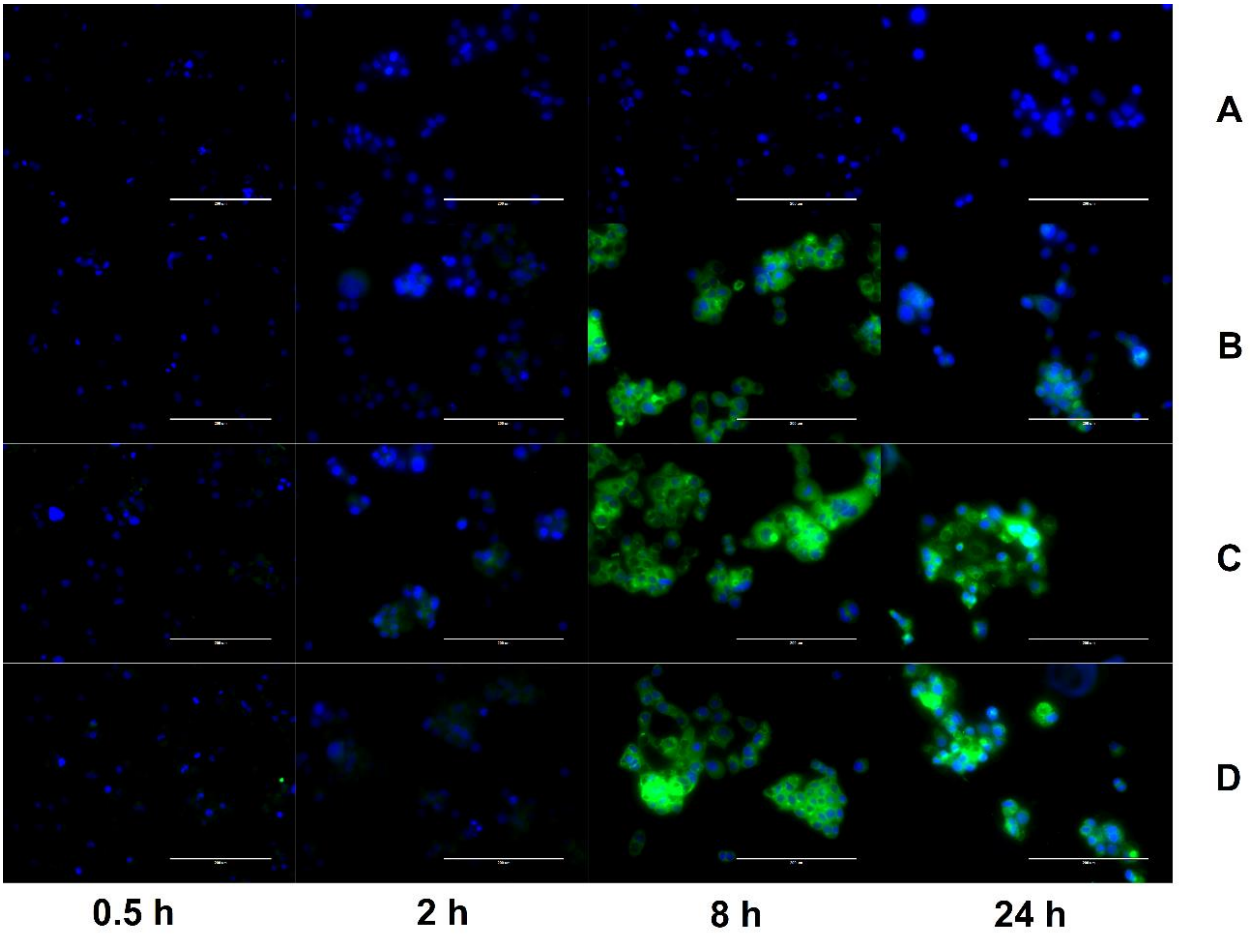

Figure 3-13: FLR microscopy of uptake of Coumarin-6 fluorescent dye (green) by OVCAR-3 cells. Cells incubated in cell medium with Coumarin-6 encapsulated PLGA NPs for up to 24 h. Cell nuclei stained with DAPI (blue) to contrast. Groups A-D: {A-free Coumarin-6 (control); B-PLGA NP; C-PLGA-COS NP; D-PLGA-COS-RGD NP}. White bar in each image represents 200 µm.

In retrospect, this uptake study was the most flawed aspect of the project. The fluorescent microscopy of the cells successfully up-taking the Coumarin-6 fluorescent model dye was useful as a visual indicator. Paired with the DAPI nuclei stains, it strongly indicated that any remaining dye after washing of the plate wells was only present inside or adsorbed at the surface of the cells. This should, however, have served as a qualitative confirmation. There were potential biases of having to manually choose images and cells, as well as several issues and limitations with the images themselves. While cells were randomly chosen to quantitate the average fluorescence signal, and 5 cells were sampled instead of the standard 3, the images themselves were taken with a certain level of bias in favour of a relatively densely populated area of cells with both visible DAPI and Coumarin-6 fluorescence. While this visually allows a clearer picture to compare the different treatment groups, it's also possible that these areas of higher cell density could also be up-taking the dye at a different rate. Another point of contention was that, in order to generate a set of images that effectively showed the uptake and presence of Coumarin-6 dye within the first few hours of incubation with the NPs, this required an initial concentration of dye that resulted in some cells, after the full 24 h incubation period, containing an amount of dye that reached or exceeded the saturation levels of some pixels. This oversaturation clearly led to artefact formation and pixel bleeding, shown in Figure 3-14. In a similar vein, the OVCAR-3 cells grow in clusters, and in some cases, appear to contain some levels of overlap. This may contribute to pixel saturation, as multiple cells that have uptaken a high level of dye could overlap and cause oversaturation.

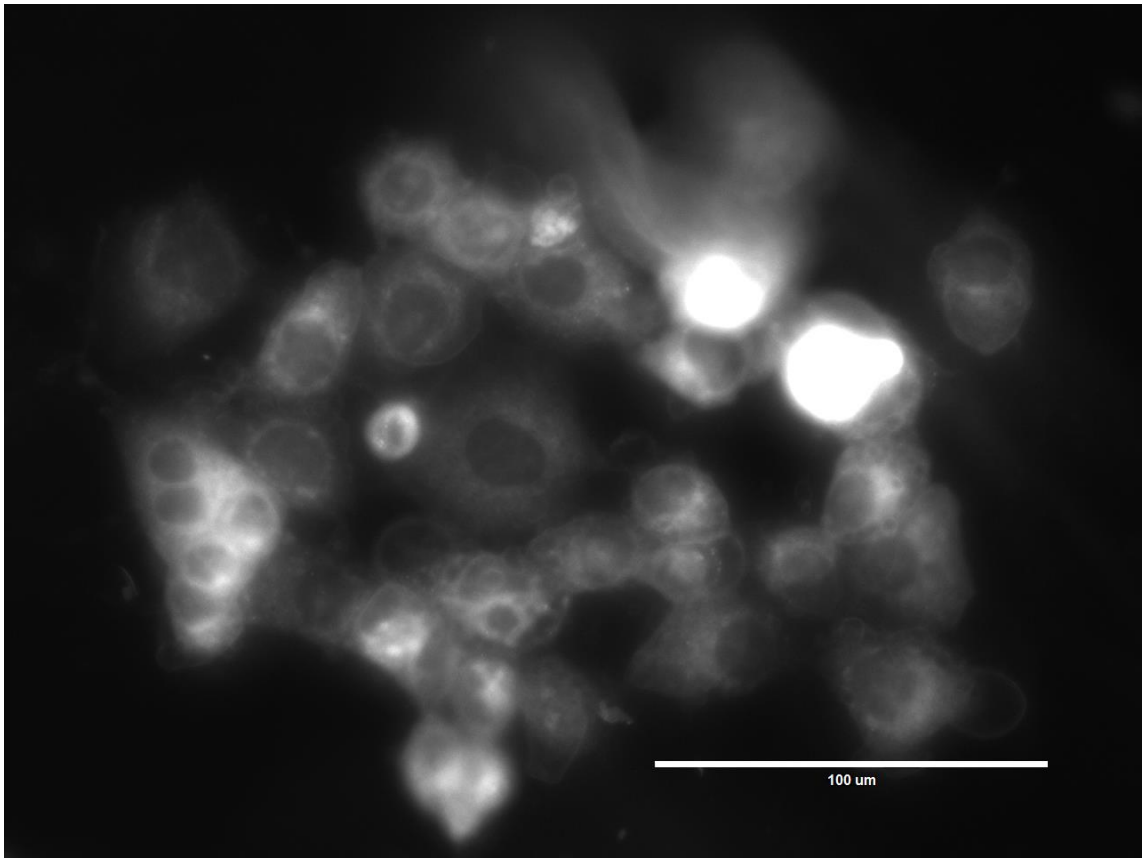

Figure 3-14: Greyscale translation of FLR microscopy a sample of OVCAR-3 cells, Coumarin-6 fluorescence only. Two cells clearly showing oversaturation, appear to bleed into adjacent pixels.

If this avenue was explored once more, a more accurate method could be to use fluorescence measurement via plate reader. Firstly, this would allow an overall picture of entire wells, instead of snapshots of individual clusters of cells via microscopy. This would also allow the use and detection of lower concentrations of dye, likely avoiding potential issues with oversaturating signal at higher dye concentrations. While cell counts, and possibly viability, would vary between samples and wells, the use of the DAPI stain could provide some level of normalization. The main issue with this would be that non-viable cells would need to be removed prior to the DAPI staining protocol (DAPI penetrates through live cells relatively poorly). Other cell viability assays could be explored, but they would need to avoid any fluorescence overlap with the Coumarin-6 dye. While absolute quantification via standard curves would

not be viable, it would still provide a relative quantification of the amount and rate of uptake of NPs via the model dye.

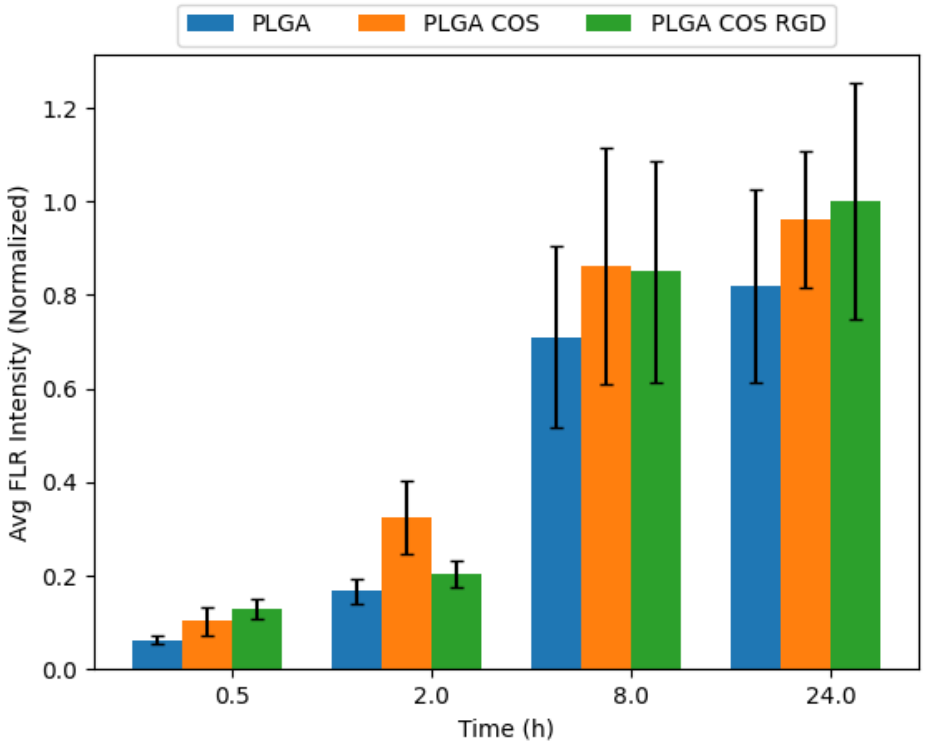

Figure 3-15: Mean Coumarin-6 fluorescent intensity values of OVCAR-3 cells treated with Coumarin-6 encapsulated NPs. Values extracted from FLR microscopy images using ImageJ analysis software.

3.5 Cell Toxicity Study

OVCAR-3 cells were treated with CUR-loaded NPs at varying concentrations from 2.5 to 40 µg/mL (shown in Figure 3-16). The 3 treatment groups of PLGA NP, PLGA-COS NP, PLGA-COS-RGD NP were compared to each other and a positive control group of free, unencapsulated CUR. Statistical analysis (ANOVA) of MTS assay indicate that change in cytotoxicity with free (unencapsulated) CUR is not statistically significant between low and high concentrations of CUR. Comparison of NP-encapsulated CUR treated samples via ANOVA and Tukey's test indicate significant difference in cytotoxicity with

increasing CUR concentration. In all NP treatment groups, cytotoxicity was not significant below 5 µg/mL, and did not show further increase of cytotoxicity above 20 µg/mL. IC50 (half-max inhibitory concentration) for all NP treatment groups appears to fall between 10-20 µg/mL (generally closer to 10); ANOVA between the three NP treatment groups did not show significant difference in their cytotoxicity at any given concentration level. Figure 3-17 shows statistical analysis between differing concentrations in a given treatment group. Each group except for the free CUR control group indicates that there is a difference in cytotoxicity with dose; in the 3 NP treatments, more than 5 µg/mL CUR is required for a statistical cytotoxic effect, while cytotoxicity does not meaningfully increase beyond 20 µg/mL CUR.

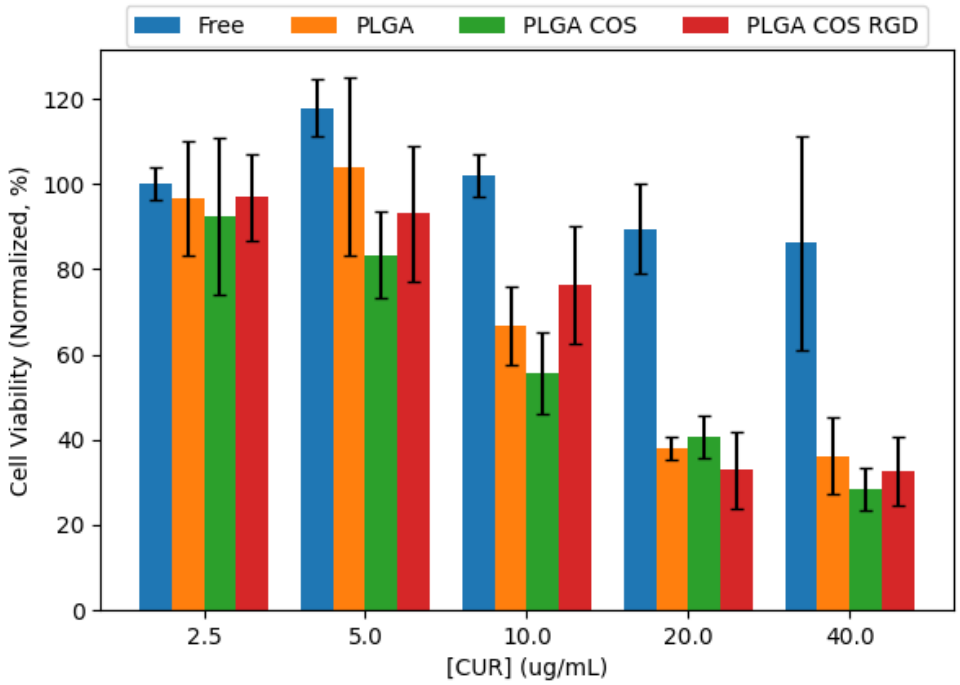

Figure 3-16: Cell viability of 24h treatment of OVCAR-3 cells at varying [CUR] (2.5 to 40 µg/mL) with MTS assay.

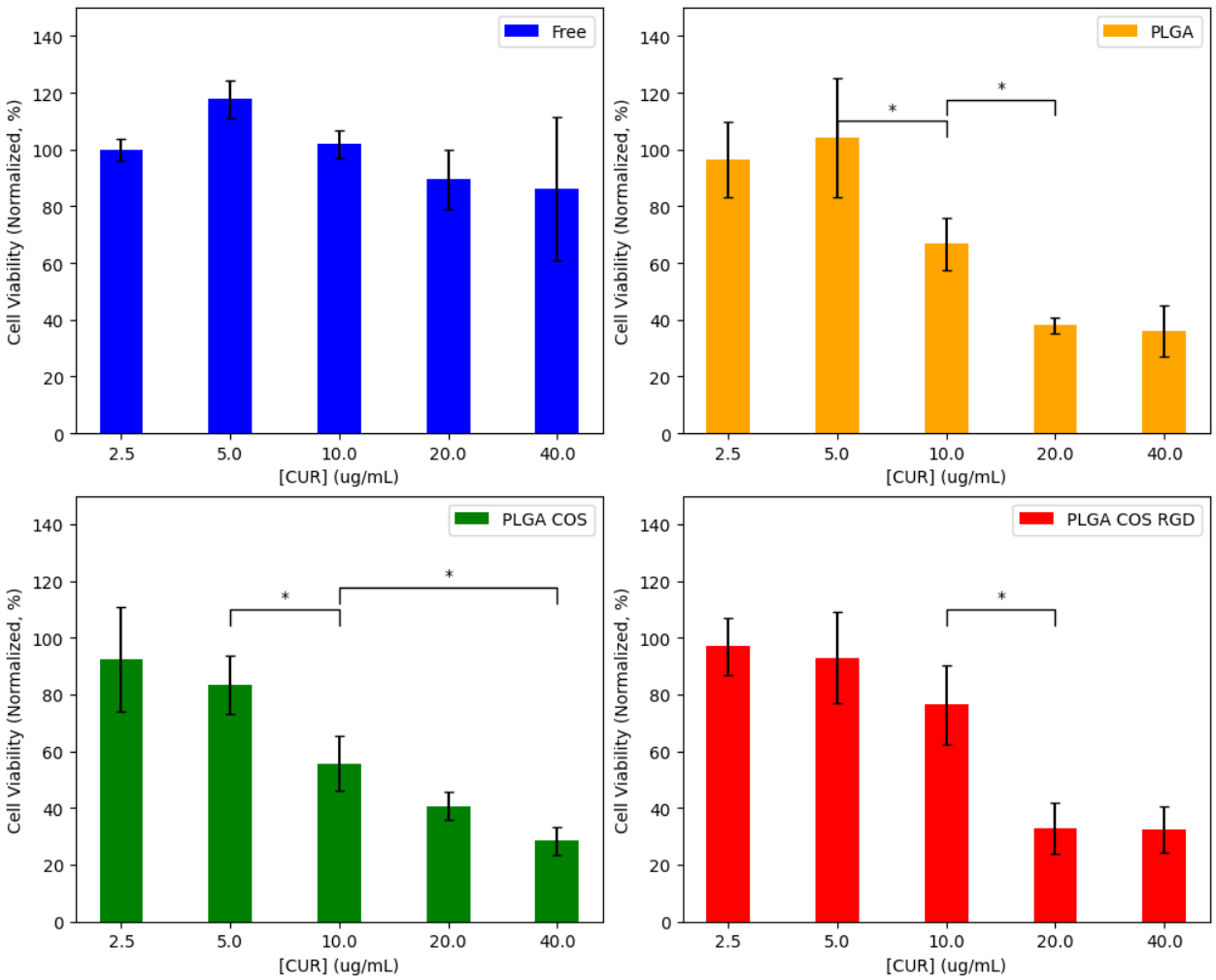

Figure 3-17: Statistical analysis of each treatment group. 95% CI (α = 0.05). (*) denotes comparison between two concentrations where {p < 0.05}. Any adjacent concentrations without explicit comparison are assumed to be "ns" {p > 0.05}.

OVCAR-3 cells were then treated at various with CUR-loaded NPs for up to 24 h, at a concentration of 40 µg/mL based on the results from Figure 3-16. As shown in Figure 3-18, significant cytotoxicity begins to occur after 8 h. At this concentration, cell viability appears to reach 50% around the 16 h mark. Again, free CUR does not appear to have statistically significant effect on the cells without the assistance of the NP delivery.

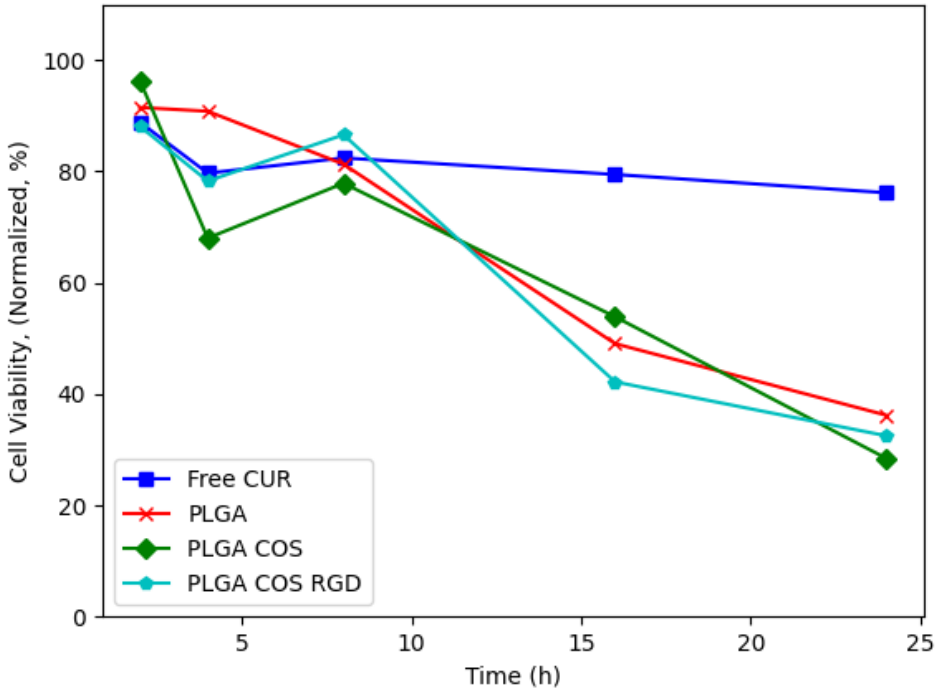

Figure 3-18: Normalized cell viability of time-dependent treatment of OVCAR-3 cells with CUR-loaded NPs (40 µg/mL CUR) at t = {2,4,8,16,24} h.

To control for the effects of only CUR and rule out cytotoxic effects from the NP itself, OVCAR-3 cells were treated with void NPs over 24 h, shown in Figure 3-19. Each treatment group had a low and high treatment concentration, corresponding respectively to the lowest and highest concentration of CUR-loaded NPs used in Figure 3-16. Statistical t-test analysis of the treatment groups did not find any statistically significant difference between high and low concentration samples. The void NPs themselves do not appear to contribute to the cytotoxicity of the CUR treatment.

Together, these results, along with the fluorescent imaging of Coumarin-6 uptake indicates that, on its own, free CUR is unable to affect cell viability, most likely due to its insolubility in aqueous medium. The NPs themselves do not appear to have cytotoxic effects, but are shown to be successfully uptaken by cells;

when CUR is encapsulated in these NPs, the CUR is successfully uptaken by cells, facilitated by the NPs. Once in the cells, the CUR exhibits cytotoxicity to the cancer cells.

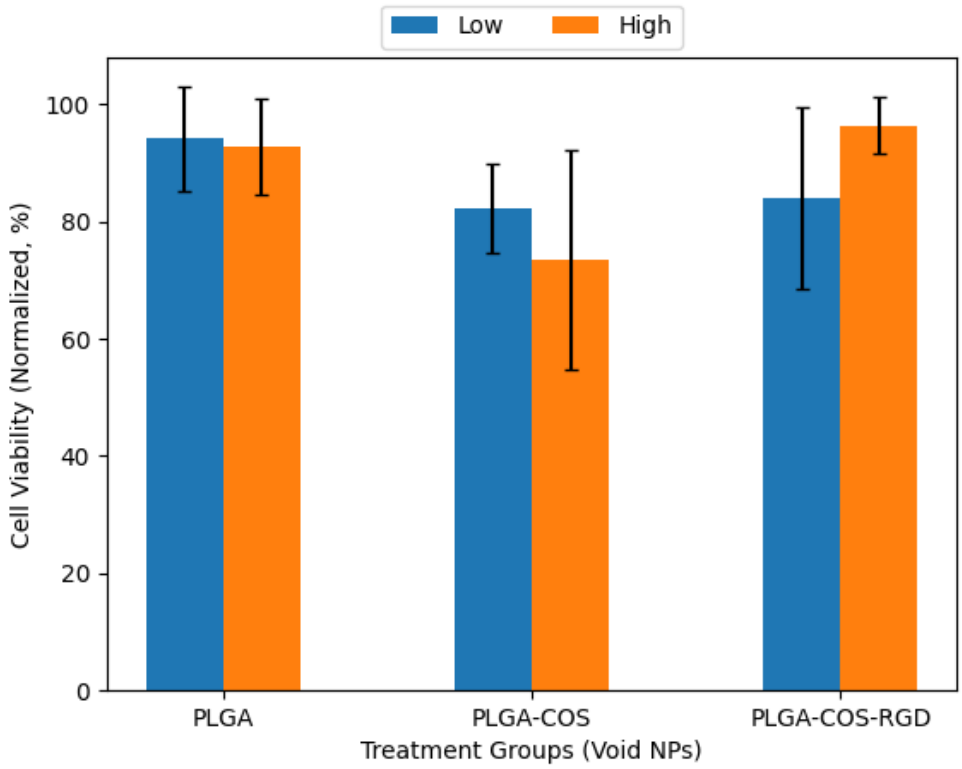

Figure 3-19: Normalized cell viability of 24h treatment of OVCAR-3 cells with void NPs. Low and high concentrations of void NPs correspond to 5 and 40 μg/mL CUR concentration if the NPs were loaded with CUR.

One of the biggest challenges to these cell viability studies was dealing with variance between samples within a given control group. Even within some control sample groups, MTS signal from the assay varied in range by as much as 30% (N = 6). Several steps were taken to mitigate potential variance, including: aspirating the cell solution several times before depositing into wells to maximize even cell dispersion, depositing cells w/ multichannel pipette column-wise but setting up replicates row-wise to avoid replicating variance due to the multichannel pipette, avoiding excess movements of the well plates during initial deposition before cell adhesion to minimize risk of uneven cell clumping/clustering. It is likely that, to

counteract the inherent sensitivity and variance of this type of study, a higher replicate count ($N \geq 6$) would be preferable in future explorations.

Though cell studies overall did not show statistically significant differences between treatment groups of PLGA, PLGA-COS and PLGA-COS-RGD NPs, it is possible that an exploration into in vitro studies comparing healthy mammalian cells to tumour cells like OVCAR-3 could yield interesting results. The coating process requires further optimization, but the coating process may assist to some degree in avoiding uptake by healthy cells in addition to targeting tumour cells via their receptors.

4 Conclusion

In this study, CUR was encapsulated in PLGA NPs. The NPs were successfully coated with COS, providing the nanocarrier with a positively charged surface. COS was successfully synthesized by depolymerization of chitosan, and stoichiometrically controlled by the molar ratio of GlcN units to nitrous acid, confirmed by ^{1}H NMR. Exploring COS size distribution via MALDI-TOF MS had limitations, as the chitosan was only partially de-acetylated, resulting in variance of MW from oligomers of the same length based on the different monomer weights of acetylated or de-acetylated GlcN units.

PLGA NPs were successfully synthesized through the emulsion method within acceptable size range (sub-500 nm diameter), and narrow distribution. EE% of CUR was 60%, which was 10% lower than similar studies observed in literature; this may be due in part to minor degradation during processing and/or storage of the NPs. NP size can be further tailored by changing various synthesis parameters, to suit various applications (i.e. location of treatment). While ZP indicated successful coating of COS, by showing a transition from significantly negative surface charge without the COS coating to significantly positive charge with the coating, this could not be validated by ^{1}H NMR. Significant solubility issues between PLGA and chitosan likely played a major role in NMR failing to register a chitosan signal when PLGA-COS NPs were dissolved in various organic solvents. The NP surface was further modified by chemical addition of RGD peptide, though binding efficiency was less than 15%. Further optimization of the binding process should be explored, including optimizing buffer and pH conditions, and the choice of alternative RGD-mimetics. Coating of COS and RGD were among the biggest challenges in this aspect of the project; in addition to needing to optimize reaction conditions, it would be important to find other methods (both direct or indirect) that can provide more concrete data for whether binding is successful.

The NP-encapsulated CUR showed significant resistance to degradation in buffered aqueous conditions compared to free, unencapsulated CUR. However, under sink conditions, it was shown that, contrary to several prior studies on the release of CUR from PLGA NPs, which showed apparent prolonged and steady release over the course of several days, PLGA NPs would release CUR within a few hours. CUR

did appear to release slowly when in a highly saturated solution; however, it is more likely that CUR in the NPs releases into the solution as CUR already in solution is degraded. It is likely that the claim of steady, linear release is predicated on the constant refreshing of fresh new medium after each time interval, allowing the NPs to release their load until saturation. When performed at equal 24 h time intervals, this makes the NPs appear to release slowly, at a linear rate, over a prolonged period. Another challenge related to CUR degradation is the fact that curcuminoid derivatives (like demethoxycurcumin and bisdemethoxycurcumin) and degradation products were extremely difficult to detect in solution, even through analysis as sensitive and selective as UPLC.

Cell uptake studies using fluorescent microscopy and NPs containing Coumarin-6 dye showed the PLGA NP ability to successfully deliver the encapsulated hydrophobic dye to OVCAR-3 cells, compared to unencapsulated Coumarin-6 control, which was unable to uptake at all even after 24 h incubation. In the future, while fluorescent microscopy provides strong qualitative results via direct imaging, fluorescent plate reader data should be gathered in tandem to provide more accurate quantitative results than manual image processing. In cell toxicity studies, OVCAR-3 cancer cells treated with encapsulated CUR showed significant toxicity to cells when compared to free CUR. Void NP treatment was used to control for toxic effects from the NP material itself; cytotoxic effects from those samples were statistically insignificant. Free CUR did not appear to show statistically significant cytotoxic effects even at concentrations where the encapsulated CUR treatments experienced cell viability well below 50%. Overall, these results show the effectiveness of PLGA-based NPs in encapsulating, stabilizing, and delivering a hydrophobic, water-sensitive drug like CUR. Lack of statistical differentiation between PLGA NPs coated with COS and RGD suggest those coating processes require further optimization. Consistency and precision were also recurring issues regarding cell studies; even among the control replicates, there was a relatively wide variance. Further in vitro studies can be performed to compare uptake of NPs and cell viability after treatment by mammalian tumour cells vs healthy mammalian cells. A caveat and limitation to these cell studies is that cytotoxicity is assumed to be entirely the result of CUR; without the ability to properly detect and separate

CUR from other curcuminoids, their cytotoxicity must be evaluated as a whole, with the assumption that CUR is the major factor in cytotoxicity based on a wealth of prior literature as well as it making up at least 80% of the curcuminoid mixture based on supplier specifications.

Overall, the project was successful in synthesizing CUR-encapsulating PLGA NPs using the emulsion method. The COS and RGD coatings showed some success, though further optimization is required, and there are issues with characterization that need to be addressed to fully confirm the coating process is successful. Cell studies showed that the NPs did vastly improve delivery of drug, but differences between PLGA, PLGA-COS and PLGA-COS-RGD NPs were inconclusive.

Further optimization will be required to improve properties such as peptide binding; there may also be avenues to explore such as the use of click chemistry in chemical binding, as well as other polymers suited for applications like anti-bacterial activity. In addition to in vitro studies, in vivo studies might help determine how effectively the NPs can target tumours, and whether they will remain in the circulatory system for prolonged periods. In vivo studies may provide a more accurate assessment of whether the nanocarrier system can preferentially target tumour cells; with in vitro tumour cell studies, the cells likely uptake the NPs that are present in the treatment more quickly than healthy cells, and the well plate nature of the treatment means that the tumour cells likely absorb as much of the NPs as they require. On the other hand, with in vivo studies, the NPs will be circulating but at much lower overall concentration, which likely means that treatment will be more reliant on the rate of uptake. One way to measure effectiveness of treatment would be by measuring relative tumour sizes over a course of treatments.[133] A major challenge to in vivo studies will be tracking NP concentrations in the bloodstream, but also accumulation in tumour tissue vs healthy tissue or potentially organs such as the kidneys/liver. While tracking drug in the bloodstream might utilise a similarly fluorescent dye in place of (or alongside) CUR, accumulation of the NPs in different tissue could require a different solution. Manual biopsy and processing of tissue might be effective to determine concentrations in specific organs and obvious tumour tissue, but it may be less effective if the NPs/drugs are accumulating in other tissue like fat. Whole body fluorescence imaging has

been used in mouse models to image distribution patterns of NP accumulation and could be used to determine whether NPs are accumulating in expected (or unexpected) locations in the body.[134,135]

Though research into NP-based solutions for drug delivery are becoming more popular, the field is still relatively new, and markets have not seen much widespread adoption of these technologies. It is hoped that this project will serve as a significant step towards the scalability and modularity that will enable the wider applicability and production of nanocarriers to enhance drug delivery and effectiveness. While this project focused on anti-cancer applications, there are numerous other potential areas of use, including anti-bacterial/anti-fungal agents, or delivery to areas of the body with otherwise low accumulation such as the past the blood-brain-barrier.

References

(1) Sung, H. et al. Global Cancer Statistics 2020: GLOBOCAN Estimates of Incidence and Mortality Worldwide for 36 Cancers in 185 Countries. *CA. Cancer J. Clin.* **2021**, *71* (3), 209–249. https://doi.org/10.3322/caac.21660.

(2) Brenner, D. R. et al. Projected Estimates of Cancer in Canada in 2022. *Can. Med. Assoc. J.* **2022**, *194* (17), E601–E607. https://doi.org/10.1503/cmaj.212097.

(3) Liang, X.-J. et al. Circumventing Tumor Resistance to Chemotherapy by Nanotechnology. In *Multi-Drug Resistance in Cancer*; Zhou, J., Ed.; Methods in Molecular Biology; Humana Press: Totowa, NJ, 2010; Vol. 596, pp 467–488. https://doi.org/10.1007/978-1-60761-416-6_21.

(4) Kennealey, G. T.; Mitchell, M. S. Factors That Influence the Therapeutic Response. In *Chemotherapy*; Becker, F. F., Ed.; Springer US: Boston, MA, 1977; pp 3–27. https://doi.org/10.1007/978-1-4615-6628-1_1.

(5) Shaw, M. T.; Stebbins, R. D. Adjunctive Chemotherapy. In *Chemotherapy*; Becker, F. F., Ed.; Springer US: Boston, MA, 1977; pp 145–162. https://doi.org/10.1007/978-1-4615-6628-1_5.

(6) Milo, R.; Phillips, R. *Cell Biology by the Numbers*; Garland Science, Taylor & Francis Group: New York, NY, 2016.

(7) Priestman, T. J. Principles of Tumour Growth. In *Cancer Chemotherapy: an Introduction*; Springer London: London, 1989; pp 3–14. https://doi.org/10.1007/978-1-4471-1686-8_1.

(8) Priestman, T. J. Biological Response Modifiers. In *Cancer Chemotherapy: an Introduction*; Springer London: London, 1989; pp 121–128. https://doi.org/10.1007/978-1-4471-1686-8_10.

(9) Priestman, T. The Theoretical Basis of Cancer Chemotherapy. In *Cancer Chemotherapy in Clinical Practice*; Springer London: London, 2008; pp 1–34. https://doi.org/10.1007/978-1-84628-991-0_1.

(10) Niculescu-Duvăz, I. et al. Alkylating Agents. In *The Chemistry of Antitumour Agents*; Wilman, D. E. V., Ed.; Springer Netherlands: Dordrecht, 1990; pp 63–130. https://doi.org/10.1007/978-94-009-0397-5_3.

(11) Davies, S. M. Therapy-Related Leukemia Associated with Alkylating Agents. *Med. Pediatr. Oncol.* **2001**, *36* (5), 536–540. https://doi.org/10.1002/mpo.1126.

(12) Vaughan, K. Triazenes. In *The Chemistry of Antitumour Agents*; Wilman, D. E. V., Ed.; Springer Netherlands: Dordrecht, 1990; pp 159–186. https://doi.org/10.1007/978-94-009-0397-5_5.

(13) Priestman, T. J. The Pharmacology of Cytotoxic Drugs. In *Cancer Chemotherapy: an Introduction*; Springer London: London, 1989; pp 27–51. https://doi.org/10.1007/978-1-4471-1686-8_3.

(14) Lugano, R. et al. Tumor Angiogenesis: Causes, Consequences, Challenges and Opportunities. *Cell. Mol. Life Sci.* **2020**, *77* (9), 1745–1770. https://doi.org/10.1007/s00018-019-03351-7.

(15) Cadman, E. Toxicity of Chemotherapeutic Agents. In *Chemotherapy*; Becker, F. F., Ed.; Springer US: Boston, MA, 1977; pp 59–111. https://doi.org/10.1007/978-1-4615-6628-1_3.

(16) Chidambaram, M. et al. Nanotherapeutics to Overcome Conventional Cancer Chemotherapy Limitations. *J. Pharm. Pharm. Sci.* **2011**, *14* (1), 67. https://doi.org/10.18433/J30C7D.

(17) Anand, P. et al. Curcumin and Cancer: An "Old-Age" Disease with an "Age-Old" Solution. *Cancer Lett.* **2008**, *267* (1), 133–164. https://doi.org/10.1016/j.canlet.2008.03.025.

(18) Wang, M. et al. Potential Mechanisms of Action of Curcumin for Cancer Prevention: Focus on Cellular Signaling Pathways and miRNAs. *Int. J. Biol. Sci.* **2019**, *15* (6), 1200–1214. https://doi.org/10.7150/ijbs.33710.

(19) Akl, M. A. et al. Factorial Design Formulation Optimization and in Vitro Characterization of Curcumin-Loaded PLGA Nanoparticles for Colon Delivery. *J. Drug Deliv. Sci. Technol.* **2016**, *32*, 10–20. https://doi.org/10.1016/j.jddst.2016.01.007.

(20) Tomeh, M. et al. A Review of Curcumin and Its Derivatives as Anticancer Agents. *Int. J. Mol. Sci.* **2019**, *20* (5), 1033. https://doi.org/10.3390/ijms20051033.

(21) Bayet-Robert, M. et al. Phase I Dose Escalation Trial of Docetaxel plus Curcumin in Patients with Advanced and Metastatic Breast Cancer. *Cancer Biol. Ther.* **2010**, *9* (1), 8–14. https://doi.org/10.4161/cbt.9.1.10392.

(22) Kanai, M. et al. A Phase I/II Study of Gemcitabine-Based Chemotherapy plus Curcumin for Patients with Gemcitabine-Resistant Pancreatic Cancer. *Cancer Chemother. Pharmacol.* **2011**, *68* (1), 157–164. https://doi.org/10.1007/s00280-010-1470-2.

(23) Cruz–Correa, M. et al. Combination Treatment With Curcumin and Quercetin of Adenomas in Familial Adenomatous Polyposis. *Clin. Gastroenterol. Hepatol.* **2006**, *4* (8), 1035–1038. https://doi.org/10.1016/j.cgh.2006.03.020.

(24) Biernat, W. et al. Alterations of Cell Cycle Regulatory Genes in Primary (de Novo) and Secondary Glioblastomas. *Acta Neuropathol. (Berl.)* **1997**, *94* (4), 303–309. https://doi.org/10.1007/s004010050711.

(25) Chiu. The Anti-Cancer Efficacy of Curcumin Scrutinized through Core Signaling Pathways in Glioblastoma. *Int. J. Mol. Med.* **2010**, *26* (2). https://doi.org/10.3892/ijmm_00000455.

(26) Gong, H. et al. P53/microRNA-374b/AKT1 Regulates Colorectal Cancer Cell Apoptosis in Response to DNA Damage. *Int. J. Oncol.* **2017**, *50* (5), 1785–1791. https://doi.org/10.3892/ijo.2017.3922.

(27) Dang, Y.-P. et al. Curcumin Improves the Paclitaxel-Induced Apoptosis of HPV-Positive Human Cervical Cancer Cells via the NF-κB-P53-Caspase-3 Pathway. *Exp. Ther. Med.* **2015**, *9* (4), 1470–1476. https://doi.org/10.3892/etm.2015.2240.

(28) Burge, K. et al. Curcumin and Intestinal Inflammatory Diseases: Molecular Mechanisms of Protection. *Int. J. Mol. Sci.* **2019**, *20* (8), 1912. https://doi.org/10.3390/ijms20081912.

(29) Kujundžić, R. et al. Curcumin and Its Potential for Systemic Targeting of Inflamm-Aging and Metabolic Reprogramming in Cancer. *Int. J. Mol. Sci.* **2019**, *20* (5), 1180. https://doi.org/10.3390/ijms20051180.

(30) Bachmeier, B.; Melchart, D. Therapeutic Effects of Curcumin—From Traditional Past to Present and Future Clinical Applications. *Int. J. Mol. Sci.* **2019**, *20* (15), 3757. https://doi.org/10.3390/ijms20153757.

(31) Chen, J. et al. Fabrication and Evaluation of Curcumin-Loaded Nanoparticles Based on Solid Lipid as a New Type of Colloidal Drug Delivery System. *Indian J. Pharm. Sci.* **2013**, *75* (2), 178–184.

(32) Senez, V. et al. *Nanotechnologies for Synthetic Super Non-Wetting Surfaces: Senez/Nanotechnologies for Synthetic Super Non-Wetting Surfaces*; John Wiley & Sons, Inc.: Hoboken, NJ, USA, 2014. https://doi.org/10.1002/9781119015093.

(33) Cao, K. et al. Elastic Straining of Free-Standing Monolayer Graphene. *Nat. Commun.* **2020**, *11* (1), 284. https://doi.org/10.1038/s41467-019-14130-0.

(34) Gahlawat, G.; Choudhury, A. R. A Review on the Biosynthesis of Metal and Metal Salt Nanoparticles by Microbes. *RSC Adv.* **2019**, *9* (23), 12944–12967. https://doi.org/10.1039/C8RA10483B.

(35) Bozzuto, G.; Molinari, A. Liposomes as Nanomedical Devices. *Int. J. Nanomedicine* **2015**, 975. https://doi.org/10.2147/IJN.S68861.

(36) Naves, L. et al. Poly(Lactic-Co-Glycolic) Acid Drug Delivery Systems through Transdermal Pathway: An Overview. *Prog. Biomater.* **2017**, *6*, 1–11. https://doi.org/10.1007/s40204-017-0063-0.

(37) Alexis, F. et al. Factors Affecting the Clearance and Biodistribution of Polymeric Nanoparticles. *Mol. Pharm.* **2008**, *5* (4), 505–515. https://doi.org/10.1021/mp800051m.

(38) Ding, S. et al. Microfluidic Nanoprecipitation Systems for Preparing Pure Drug or Polymeric Drug Loaded Nanoparticles: An Overview. *Expert Opin. Drug Deliv.* **2016**, *13* (10), 1447–1460. https://doi.org/10.1080/17425247.2016.1193151.

(39) Eley, J. G. et al. Poly (Lactide-Co-Glycolide) Nanoparticles Containing Coumarin-6 for Suppository Delivery: In Vitro Release Profile and In Vivo Tissue Distribution. *Drug Deliv.* **2004**, *11* (4), 255–261. https://doi.org/10.1080/10717540490467384.

(40) McCall, R. L.; Sirianni, R. W. PLGA Nanoparticles Formed by Single- or Double-Emulsion with Vitamin E-TPGS. *JoVE J. Vis. Exp.* **2013**, No. 82, e51015. https://doi.org/10.3791/51015.

(41) Deng, M. et al. Modification of PLGA Scaffold by MSC-Derived Extracellular Matrix Combats Macrophage Inflammation to Initiate Bone Regeneration via TGF- β -Induced Protein. *Adv. Healthc. Mater.* **2020**, *9* (13), 2000353. https://doi.org/10.1002/adhm.202000353.

(42) Shen, X. et al. PLGA-Based Drug Delivery Systems for Remotely Triggered Cancer Therapeutic and Diagnostic Applications. *Front. Bioeng. Biotechnol.* **2020**, *8*, 381. https://doi.org/10.3389/fbioe.2020.00381.

(43) Guarecuco, R. et al. Immunogenicity of Pulsatile-Release PLGA Microspheres for Single-Injection Vaccination. *Vaccine* **2018**, *36* (22), 3161–3168. https://doi.org/10.1016/j.vaccine.2017.05.094.

(44) Sedki, M. et al. Hybrid Nanocarrier System for Guiding and Augmenting Simvastatin Cytotoxic Activity against Prostate Cancer. *Artif. Cells Nanomedicine Biotechnol.* **2018**, *46* (sup3), S641–S650. https://doi.org/10.1080/21691401.2018.1505743.

(45) Sutar, Y. B.; Telvekar, V. N. Chitosan Based Copolymer-Drug Conjugate and Its Protein Targeted Polyelectrolyte Complex Nanoparticles to Enhance the Efficiency and Specificity of Low Potency Anticancer Agent. *Mater. Sci. Eng. C* **2018**, *92*, 393–406. https://doi.org/10.1016/j.msec.2018.07.001.

(46) Xia, W. et al. Biological Activities of Chitosan and Chitooligosaccharides. *Food Hydrocoll.* **2011**, *25* (2), 170–179. https://doi.org/10.1016/j.foodhyd.2010.03.003.

(47) Dong, W. et al. Chitosan Based Polymer-Lipid Hybrid Nanoparticles for Oral Delivery of Enoxaparin. *Int. J. Pharm.* **2018**, *547* (1), 499–505. https://doi.org/10.1016/j.ijpharm.2018.05.076.

(48) Ryu, J. H. et al. Tumor-Targeting Glycol Chitosan Nanoparticles for Cancer Heterogeneity. *Adv. Mater.* **2020**, *32* (51), 2002197. https://doi.org/10.1002/adma.202002197.

(49) Mazzarino, L. et al. Xyloglucan-Block-Poly(ϵ-Caprolactone) Copolymer Nanoparticles Coated with Chitosan as Biocompatible Mucoadhesive Drug Delivery System. *Macromol. Biosci.* **2014**, *14* (5), 709–719. https://doi.org/10.1002/mabi.201300465.

(50) Moussa, A. et al. Reducing-End "Clickable" Functionalizations of Chitosan Oligomers for the Synthesis of Chitosan-Based Diblock Copolymers. *Carbohydr. Polym.* **2019**, *219*, 387–394. https://doi.org/10.1016/j.carbpol.2019.04.078.

(51) Allan, G. G.; Peyron, M. Molecular Weight Manipulation of Chitosan I: Kinetics of Depolymerization by Nitrous Acid. *Carbohydr. Res.* **1995**, *277* (2), 257–272. https://doi.org/10.1016/0008-6215(95)00207-A.

(52) Moussa, A.; Trombotto, S. Octanoic Hydrazide-Linked Chitooligosaccharides-2,5-Anhydro-d-Mannofuranose. *Molbank* **2016**, *2016* (3), M904. https://doi.org/10.3390/M904.

(53) *Adipic acid dihydrazide =98 titration 1071-93-8*. Millipore Sigma. http://www.sigmaaldrich.com/CA/en/product/sigma/a0638 (accessed 2023-08-24).

(54) Xing, Y. et al. Nanodelivery of Triamcinolone Acetonide with PLGA-Chitosan Nanoparticles for the Treatment of Ocular Inflammation. *Artif. Cells Nanomedicine Biotechnol.* **2021**, *49* (1), 308–316. https://doi.org/10.1080/21691401.2021.1895184.

(55) Wang, Y. et al. Chitosan-Modified PLGA Nanoparticles with Versatile Surface for Improved Drug Delivery. *AAPS PharmSciTech* **2013**, *14* (2), 585–592. https://doi.org/10.1208/s12249-013-9943-3.

(56) Liu, Z. et al. Integrin Avβ3-Targeted Cancer Therapy. *Drug Dev. Res.* **2008**, *69* (6), 329–339. https://doi.org/10.1002/ddr.20265.

(57) Avraamides, C.; Varner, J. Fibronectins and Their Receptors in Cancer. In *Cell-extracellular matrix interactions in cancer*; Zent, R., Pozzi, A., Eds.; Springer: New York, 2010; pp 111–136.

(58) Deford, P. et al. MAGP2 Controls Notch via Interactions with RGD Binding Integrins: Identification of a Novel ECM–Integrin–Notch Signaling Axis. *Exp. Cell Res.* **2016**, *341* (1), 84–91. https://doi.org/10.1016/j.yexcr.2016.01.011.

(59) Schottelius, M. et al. Ligands for Mapping Avβ3-Integrin Expression in Vivo. *Acc. Chem. Res.* **2009**, *42* (7), 969–980. https://doi.org/10.1021/ar800243b.

(60) Tan, H. et al. RGD Modified PLGA/Gelatin Microspheres as Microcarriers for Chondrocyte Delivery. *J. Biomed. Mater. Res. B Appl. Biomater.* **2009**, *91B* (1), 228–238. https://doi.org/10.1002/jbm.b.31394.

(61) Xiong, X.-B. et al. The Therapeutic Response to Multifunctional Polymeric Nano-Conjugates in the Targeted Cellular and Subcellular Delivery of Doxorubicin. *Biomaterials* **2010**, *31* (4), 757–768. https://doi.org/10.1016/j.biomaterials.2009.09.080.

(62) Xiong, X.-B. et al. Multifunctional Polymeric Micelles for Enhanced Intracellular Delivery of Doxorubicin to Metastatic Cancer Cells. *Pharm. Res.* **2008**, *25* (11), 2555–2566. https://doi.org/10.1007/s11095-008-9673-5.

(63) Mu, L.; Feng, S. S. Fabrication, Characterization and in Vitro Release of Paclitaxel (Taxol®) Loaded Poly (Lactic-Co-Glycolic Acid) Microspheres Prepared by Spray Drying Technique with Lipid/Cholesterol Emulsifiers. *J. Controlled Release* **2001**, *76* (3), 239–254. https://doi.org/10.1016/S0168-3659(01)00440-0.

(64) Liu, Y. et al. Formulation of Nanoparticles Using Mixing-Induced Nanoprecipitation for Drug Delivery. *Ind. Eng. Chem. Res.* **2020**, *59* (9), 4134–4149. https://doi.org/10.1021/acs.iecr.9b04747.

(65) Khalil, N. M. et al. Pharmacokinetics of Curcumin-Loaded PLGA and PLGA–PEG Blend Nanoparticles after Oral Administration in Rats. *Colloids Surf. B Biointerfaces* **2013**, *101*, 353–360. https://doi.org/10.1016/j.colsurfb.2012.06.024.

(66) Trenkenschuh, E.; Friess, W. Freeze-Drying of Nanoparticles: How to Overcome Colloidal Instability by Formulation and Process Optimization. *Eur. J. Pharm. Biopharm.* **2021**, *165*, 345–360. https://doi.org/10.1016/j.ejpb.2021.05.024.

(67) Saez, A. et al. Freeze-Drying of Polycaprolactone and Poly(d,l -Lactic-Glycolic) Nanoparticles Induce Minor Particle Size Changes Affecting the Oral Pharmacokinetics of Loaded Drugs. *Eur. J. Pharm. Biopharm.* **2000**, *50* (3), 379–387. https://doi.org/10.1016/S0939-6411(00)00125-9.

(68) Fonte, P. et al. Effect of Cryoprotectants on the Porosity and Stability of Insulin-Loaded PLGA Nanoparticles after Freeze-Drying. *Biomatter* **2012**, *2* (4), 329–339. https://doi.org/10.4161/biom.23246.

(69) Yadav, K. S.; Sawant, K. K. Modified Nanoprecipitation Method for Preparation of Cytarabine-Loaded PLGA Nanoparticles. *AAPS PharmSciTech* **2010**, *11* (3), 1456–1465. https://doi.org/10.1208/s12249-010-9519-4.

(70) Jin, M. et al. Smart Polymeric Nanoparticles with pH-Responsive and PEG-Detachable Properties for Co-Delivering Paclitaxel and Survivin siRNA to Enhance Antitumor Outcomes. *Int. J. Nanomedicine* **2018**, *13*, 2405–2426. https://doi.org/10.2147/IJN.S161426.

(71) Gao, J. et al. Co-Delivery of Docetaxel and Salinomycin to Target Both Breast Cancer Cells and Stem Cells by PLGA/TPGS Nanoparticles. *Int. J. Nanomedicine* **2019**, *14*, 9199–9216. https://doi.org/10.2147/IJN.S230376.

(72) Ahmad, N. et al. Enhancement of Oral Bioavailability of Doxorubicin through Surface Modified Biodegradable Polymeric Nanoparticles. *Chem. Cent. J.* **2018**, *12*, 65. https://doi.org/10.1186/s13065-018-0434-1.

(73) Khanna, V. et al. Perlecan-Targeted Nanoparticles for Drug Delivery to Triple-Negative Breast Cancer. *Future Drug Discov. 1* (1), FDD8. https://doi.org/10.4155/fdd-2019-0005.

(74) Cırpanlı, Y. et al. Antitumoral Activity of Camptothecin-Loaded Nanoparticles in 9L Rat Glioma Model. *Int. J. Pharm.* **2011**, *403* (1–2), 201–206. https://doi.org/10.1016/j.ijpharm.2010.10.015.

(75) Guo, J. et al. Aptamer-Functionalized PEG-PLGA Nanoparticles for Enhanced Anti-Glioma Drug Delivery. *Biomaterials* **2011**, *32* (31), 8010–8020. https://doi.org/10.1016/j.biomaterials.2011.07.004.

(76) Hlaing, S. P. et al. Hyaluronic Acid-Conjugated PLGA Nanoparticles Alleviate Ulcerative Colitis via CD44-Mediated Dual Targeting to Inflamed Colitis Tissue and Macrophages. *Pharmaceutics* **2022**, *14* (10), 2118. https://doi.org/10.3390/pharmaceutics14102118.

(77) Hong, L. et al. Hyaluronic Acid (HA)-Based Hydrogels for Full-Thickness Wound Repairing and Skin Regeneration. *J. Mater. Sci. Mater. Med.* **2018**, *29* (9). https://doi.org/10.1007/s10856-018-6158-x.

(78) Chen, T. et al. Self-Assembly pH-Sensitive Chitosan/Alginate Coated Polyelectrolyte Complexes for Oral Delivery of Insulin. *J. Microencapsul.* **2019**, *36* (1), 96–107. https://doi.org/10.1080/02652048.2019.1604846.

(79) Abouelmagd, S. A. et al. Tannic Acid-Mediated Surface Functionalization of Polymeric Nanoparticles. *ACS Biomater. Sci. Eng.* **2016**, *2* (12), 2294–2303. https://doi.org/10.1021/acsbiomaterials.6b00497.

(80) Passirani, C. et al. Interactions of Nanoparticles Bearing Heparin or Dextran Covalently Bound to Poly(Methyl Methacrylate) with the Complement System. *Life Sci.* **1998**, *62* (8), 775–785. https://doi.org/10.1016/s0024-3205(97)01175-2.

(81) *Amine-Reactive Crosslinker Chemistry*. Thermo Fisher Scientific. https://www.thermofisher.com/ca/en/home/life-science/protein-biology/protein-biology-learning-

center/protein-biology-resource-library/pierce-protein-methods/amine-reactive-crosslinker-chemistry.html (accessed 2021-09-24).

(82) *Carbodiimide Crosslinker Chemistry*. Thermo Fisher Scientific. https://www.thermofisher.com/ca/en/home/life-science/protein-biology/protein-biology-learning-center/protein-biology-resource-library/pierce-protein-methods/carbodiimide-crosslinker-chemistry.html (accessed 2022-10-05).

(83) *N-(3-Dimethylaminopropyl)-N -ethylcarbodiimide crystalline 25952-53-8*. Millipore Sigma. http://www.sigmaaldrich.com/CA/en/product/sial/e7750 (accessed 2023-08-17).

(84) Thirumurugan, P. et al. Click Chemistry for Drug Development and Diverse Chemical–Biology Applications. *Chem. Rev.* **2013**, *113* (7), 4905–4979. https://doi.org/10.1021/cr200409f.

(85) Debets, M. F. et al. Aza-Dibenzocyclooctynes for Fast and Efficient Enzyme PEGylation via Copper-Free (3+2) Cycloaddition. *Chem. Commun.* **2010**, *46* (1), 97–99. https://doi.org/10.1039/B917797C.

(86) Marks, I. S. et al. Strain-Promoted "Click" Chemistry for Terminal Labeling of DNA. *Bioconjug. Chem.* **2011**, *22* (7), 1259–1263. https://doi.org/10.1021/bc1003668.

(87) Kim, K.-M. et al. Surface Treatment of Silica Nanoparticles for Stable and Charge-Controlled Colloidal Silica. *Int. J. Nanomedicine* **2014**, *9* (Suppl 2), 29–40. https://doi.org/10.2147/IJN.S57922.

(88) Vollath, D.; Szabó, D. V. Coated Nanoparticles: A New Way to Improved Nanocomposites. *J. Nanoparticle Res.* **1999**, *1* (2), 235–242. https://doi.org/10.1023/A:1010060701507.

(89) Rasmussen, M. K. et al. Size and Surface Charge Characterization of Nanoparticles with a Salt Gradient. *Nat. Commun.* **2020**, *11* (1), 2337. https://doi.org/10.1038/s41467-020-15889-3.

(90) Zielińska, A. et al. Polymeric Nanoparticles: Production, Characterization, Toxicology and Ecotoxicology. *Molecules* **2020**, *25* (16), 3731. https://doi.org/10.3390/molecules25163731.

(91) Canet, D. *Nuclear Magnetic Resonance: Concepts and Methods*; Wiley: Chichester ; New York, 1996.

(92) Sun, J. et al. Characterization of Commercial PLGAs by NMR Spectroscopy. *Drug Deliv. Transl. Res.* **2022**, *12* (3), 720–729. https://doi.org/10.1007/s13346-021-01023-3.

(93) Fleming, I.; Williams, D. *Spectroscopic Methods in Organic Chemistry*, Seventh edition.; Springer: Cham, Switzerland, 2019.

(94) Da Silva, R. M. P. et al. Straightforward Determination of the Degree of *N* -Acetylation of Chitosan by Means of First-Derivative UV Spectrophotometry: Straightforward Determination of the Degree of *N* -Acetylation of Chitosan …. *Macromol. Chem. Phys.* **2008**, *209* (14), 1463–1472. https://doi.org/10.1002/macp.200800191.

(95) Pecora, R. *Dynamic Light Scattering: Applications of Photon Correlation Spectroscopy*; Springer US: Boston, MA, 1985. https://doi.org/10.1007/978-1-4613-2389-1.

(96) McNeil-Watson, F. Electrophoretic Light Scattering. In *Encyclopedia of Biophysics*; Roberts, G. C. K., Ed.; Springer: Berlin, Heidelberg, 2013; pp 648–654. https://doi.org/10.1007/978-3-642-16712-6_288.

(97) C. Moldoveanu, S.; David, V. *Analytical Liquid Chromatography - New Perspectives*; IntechOpen, 2022. https://doi.org/10.5772/intechopen.97995.

(98) Sapan, C. V. et al. Colorimetric Protein Assay Techniques. *Biotechnol. Appl. Biochem.* **1999**, *29* (2), 99–108. https://doi.org/10.1111/j.1470-8744.1999.tb00538.x.

(99) Henry, R. J. et al. *Clinical Chemistry; Principles and Technics*, 2d ed.; Medical Dept., Harper & Row: Hagerstown, Md, 1974.

(100) Vashist, S. K.; Dixit, C. K. Interference of N-Hydroxysuccinimide with Bicinchoninic Acid Protein Assay. *Biochem. Biophys. Res. Commun.* **2011**, *411* (2), 455–457. https://doi.org/10.1016/j.bbrc.2011.06.187.

(101) Cayot, P.; Tainturier, G. The Quantification of Protein Amino Groups by the Trinitrobenzenesulfonic Acid Method: A Reexamination. *Anal. Biochem.* **1997**, *249* (2), 184–200. https://doi.org/10.1006/abio.1997.2161.

(102) Riss, T. L. et al. Cell Viability Assays. In *Assay Guidance Manual*; Markossian, S. et al., Eds.; Eli Lilly & Company and the National Center for Advancing Translational Sciences: Bethesda (MD), 2004.

(103) Berridge, M. V.; Tan, A. S. Characterization of the Cellular Reduction of 3-(4,5-Dimethylthiazol-2-Yl)-2,5-Diphenyltetrazolium Bromide (MTT): Subcellular Localization, Substrate Dependence, and Involvement of Mitochondrial Electron Transport in MTT Reduction. *Arch. Biochem. Biophys.* **1993**, *303* (2), 474–482. https://doi.org/10.1006/abbi.1993.1311.

(104) Markossian, S. et al. *Assay Guidance Manual*; Eli Lilly & Company and the National Center for Advancing Translational Sciences: Bethesda (MD), 2004.

(105) Berridge, M. V. et al. Tetrazolium Dyes as Tools in Cell Biology: New Insights into Their Cellular Reduction. In *Biotechnology Annual Review*; Elsevier, 2005; Vol. 11, pp 127–152. https://doi.org/10.1016/S1387-2656(05)11004-7.

(106) Shum, D. et al. A High Density Assay Format for the Detection of Novel Cytotoxic Agents in Large Chemical Libraries. *J. Enzyme Inhib. Med. Chem.* **2008**, *23* (6), 931–945. https://doi.org/10.1080/14756360701810082.

(107) O'Brien, J. et al. Investigation of the Alamar Blue (Resazurin) Fluorescent Dye for the Assessment of Mammalian Cell Cytotoxicity: Resazurin as a Cytotoxicity Assay. *Eur. J. Biochem.* **2000**, *267* (17), 5421–5426. https://doi.org/10.1046/j.1432-1327.2000.01606.x.

(108) Niles, A. L. et al. A Homogeneous Assay to Measure Live and Dead Cells in the Same Sample by Detecting Different Protease Markers. *Anal. Biochem.* **2007**, *366* (2), 197–206. https://doi.org/10.1016/j.ab.2007.04.007.

(109) Rafiei, P.; Haddadi, A. Docetaxel-Loaded PLGA and PLGA-PEG Nanoparticles for Intravenous Application: Pharmacokinetics and Biodistribution Profile. *Int. J. Nanomedicine* **2017**, *12*, 935–947. https://doi.org/10.2147/IJN.S121881.

(110) Dijkgraaf, I. et al. Avβ3 Integrin-Targeting of Intraperitoneally Growing Tumors with a Radiolabeled RGD Peptide. *Int. J. Cancer* **2006**, *120* (3), 605–610. https://doi.org/10.1002/ijc.22297.

(111) Takenaka, N. et al. Acceleration Mechanism of Chemical Reaction by Freezing: The Reaction of Nitrous Acid with Dissolved Oxygen. *J. Phys. Chem.* **1996**, *100* (32), 13874–13884. https://doi.org/10.1021/jp9525806.

(112) Tømmeraas, K. et al. Preparation and Characterisation of Oligosaccharides Produced by Nitrous Acid Depolymerisation of Chitosans. *Carbohydr. Res.* **2001**, *333* (2), 137–144. https://doi.org/10.1016/S0008-6215(01)00130-6.

(113) Einbu, A.; Vårum, K. M. Depolymerization and De-N-Acetylation of Chitin Oligomers in Hydrochloric Acid. *Biomacromolecules* **2007**, *8* (1), 309–314. https://doi.org/10.1021/bm0608535.

(114) Aljbour, N. D. et al. Acid Hydrolysis of Chitosan to Oligomers Using Hydrochloric Acid. *Chem. Eng. Technol.* **2019**, *42* (9), 1741–1746. https://doi.org/10.1002/ceat.201800527.

(115) Bilati, U. et al. Sonication Parameters for the Preparation of Biodegradable Nanocapsulesof Controlled Size by the Double Emulsion Method: RESEARCH ARTICLE. *Pharm. Dev. Technol.* **2003**, *8* (1), 1–9. https://doi.org/10.1081/PDT-120017517.

(116) Tadros, T. F. Emulsion Formation, Stability, and Rheology. In *Emulsion Formation and Stability*; John Wiley & Sons, Ltd, 2013; pp 1–75. https://doi.org/10.1002/9783527647941.ch1.

(117) Madani, F. et al. Investigation of Effective Parameters on Size of Paclitaxel Loaded PLGA Nanoparticles. *Adv. Pharm. Bull.* **2018**, *8* (1), 77–84. https://doi.org/10.15171/apb.2018.010.

(118) Feczkó, T. et al. Influence of Process Conditions on the Mean Size of PLGA Nanoparticles. *Chem. Eng. Process. Process Intensif.* **2011**, *50* (8), 846–853. https://doi.org/10.1016/j.cep.2011.05.006.

(119) Vandervoort, J.; Ludwig, A. Biocompatible Stabilizers in the Preparation of PLGA Nanoparticles: A Factorial Design Study. *Int. J. Pharm.* **2002**, *238* (1), 77–92. https://doi.org/10.1016/S0378-5173(02)00058-3.

(120) Murakami, H. et al. Influence of the Degrees of Hydrolyzation and Polymerization of Poly(Vinylalcohol) on the Preparation and Properties of Poly(Dl-Lactide-Co-Glycolide) Nanoparticle. *Int. J. Pharm.* **1997**, *149* (1), 43–49. https://doi.org/10.1016/S0378-5173(96)04854-5.

(121) Thevarajah, J. J. et al. Determination of the Distributions of Degrees of Acetylation of Chitosan. *Int. J. Biol. Macromol.* **2017**, *95*, 40–48. https://doi.org/10.1016/j.ijbiomac.2016.10.056.

(122) Kurita, K. et al. Solubilization of a Rigid Polysaccharide: Controlled Partial N-Acetylation of Chitosan to Develop Solubility. *Carbohydr. Polym.* **1991**, *16* (1), 83–92. https://doi.org/10.1016/0144-8617(91)90072-K.

(123) Gao, M. et al. Enhanced Curcumin Solubility and Antibacterial Activity by Encapsulation in PLGA Oily Core Nanocapsules. *Food Funct.* **2020**, *11* (1), 448–455. https://doi.org/10.1039/c9fo00901a.

(124) Jude, S. et al. Development of Validated Methods and Quantification of Curcuminoids and Curcumin Metabolites and Their Pharmacokinetic Study of Oral Administration of Complete Natural Turmeric Formulation (Cureit^{TM}) in Human Plasma via UPLC/ESI-Q-TOF-MS Spectrometry. *Mol. J. Synth. Chem. Nat. Prod. Chem.* **2018**, *23* (10), 2415. https://doi.org/10.3390/molecules23102415.

(125) Shi, M. et al. Characterization of Curcumin Metabolites in Rats by Ultra-High-Performance Liquid Chromatography with Electrospray Ionization Quadrupole Time-of-Flight Tandem Mass Spectrometry. *Rapid Commun. Mass Spectrom.* **2019**, *33* (13), 1114–1121. https://doi.org/10.1002/rcm.8450.

(126) Joseph, A. I. et al. A Curcumin Degradation Product, 7-Norcyclopentadione, Formed by Aryl Migration and Loss of a Carbon from the Heptadienedione Chain. *J. Nat. Prod.* **2018**, *81* (12), 2756–2762. https://doi.org/10.1021/acs.jnatprod.8b00822.

(127) Yallapu, M. M. et al. Fabrication of Curcumin Encapsulated PLGA Nanoparticles for Improved Therapeutic Effects in Metastatic Cancer Cells. *J. Colloid Interface Sci.* **2010**, *351* (1), 19–29. https://doi.org/10.1016/j.jcis.2010.05.022.

(128) Gutierrez, J. K. T. et al. Encapsulation of Curcumin in Polymeric Nanoparticles for Antimicrobial Photodynamic Therapy. *PLOS ONE* **2017**, *12* (11), e0187418. https://doi.org/10.1371/journal.pone.0187418.

(129) Kurien, B. T.; Scofield, R. H. Increasing Aqueous Solubility of Curcumin for Improving Bioavailability. *Trends Pharmacol. Sci.* **2009**, *30* (7), 334–335. https://doi.org/10.1016/j.tips.2009.04.005.

(130) Kurien, B. T. et al. Improving the Solubility and Pharmacological Efficacy of Curcumin by Heat Treatment. *Assay Drug Dev. Technol.* **2007**, *5* (4), 567–576. https://doi.org/10.1089/adt.2007.064.

(131) Górnicka, J. et al. Methods to Improve the Solubility of Curcumin from Turmeric. *Life* **2023**, *13* (1), 207. https://doi.org/10.3390/life13010207.

(132) Dong, M. W. *HPLC and UHPLC for Practicing Scientists*, Second ed.; Wiley: Hoboken, NJ, 2019.

(133) Zhang, Z. et al. Induction of Anti-Tumor Cytotoxic T Cell Responses through PLGA-Nanoparticle Mediated Antigen Delivery. *Biomaterials* **2011**, *32* (14), 3666–3678. https://doi.org/10.1016/j.biomaterials.2011.01.067.

(134) Meng, F. et al. Quantitative Assessment of Nanoparticle Biodistribution by Fluorescence Imaging, Revisited. *ACS Nano* **2018**, *12* (7), 6458–6468. https://doi.org/10.1021/acsnano.8b02881.

(135) Leblond, F. et al. Preclinical Whole-Body Fluorescence Imaging: Review of Instruments, Methods and Applications. *J. Photochem. Photobiol. B* **2010**, *98* (1), 77–94. https://doi.org/10.1016/j.jphotobiol.2009.11.007.